Effect of Monomer Structure and Compressibility on the Properties of Multicomponent Polymer Blends and Solutions: 2. Application to Binary Blends

Jacek Dudowicz, Michele S. Freed, and Karl F. Freed*

The James Franck Institute and the Department of Chemistry, University of Chicago, Chicago, Illinois 60637

Received December 4, 1990; Revised Manuscript Received February 19, 1991

ABSTRACT: The general lattice cluster theory of corrections to classic Flory-Huggins theory from paper 1 is applied to compressible binary polymer blends. The properties considered are the small-angle neutron scattering intensity and excess thermodynamic quantities, with more emphasis placed on the former because its pressure dependence has not previously been studied. We first illustrate the theory with the idealized athermal limit blend, which is of interest because it yields a pure entropic contribution to the interaction parameter from extrapolated zero-angle neutron scattering. This pure athermal limit takes all three independent van der Waals interaction energies to vanish, and our calculations show that the small-angle neutron scattering intensity displays several interesting variations with composition, pressure, molecular weights, and monomer structures. However, this idealized athermal system only yields stable one-phase, dense blends at quite elevated pressures, so it is inappropriate for real polymer blends. We therefore introduce a more realistic quasiathermal blend model in which the small-angle neutron scattering intensity is insensitive to temperature but in which van der Waals interactions are present to make the blend stable at normal conditions. We study the influence of pressure, variations of the three independent van der Waals interaction energies, molecular weights, and monomer structures on the neutron scattering and excess thermodynamic properties of nonathermal blends. Other measures of the Flory interaction parameter are obtained from the entropy of mixing (in the athermal limit), the heat of mixing, or the free energy of mixing and are shown often to depart from the behavior of the interaction parameter deduced from small-angle neutron scattering. For instance, there are examples in which the latter interaction parameter is positive, suggesting interactions that are unfavorable for blend formation, whereas the former measures are negative and correctly predict blend stability. The neutron scattering interaction parameter displays the most interesting variations with pressure, monomer structure, composition, and van der Waals interactions, while the behavior of the volume change on mixing is most in line with expectations.

I. Introduction

A wide variety of composite materials are derived from polymer blends. Composite properties are greatly affected by whether the polymers are homogeneously distributed throughout the material or whether they are microscopically phase separated. In the latter case the properties may be strongly dependent on the morphology and the nature of the interfacial profile. Some composites employ block copolymers to stabilize the one-phase region, to strengthen interfaces, or to influence the morphology of the phase-separated system. Enormous numbers of possibilities exist for combining polymers under varying physical conditions, and theoretical guidance would be helpful in synthesizing blends to meet the specifications of particular applications.

Considerable effort has been devoted to understanding the molecular basis for this interesting multitude of possible composite structures and properties. One of the major approaches involves various types of experimental determinations for the Flory interaction parameter χ_{eff}, which is then used in theories describing the thermodynamics of blends, their phase separations, and the strengths of interfacial profiles. These theories are generally based on the Flory-Huggins (FH) mean field approximation[1] or other models in which χ_{eff} is either the only empirical parameter or in which it appears as a central quantity. However, the relationship between χ_{eff} and the monomer structures and their interactions has been enormously elusive since the inception of Flory-Huggins theory almost 50 years ago. Nevertheless, there is a widespread belief that a truly molecular understanding of χ_{eff} would greatly aid in the fabrication of polymeric materials with new and enhanced properties.

Unfortunately, some reflection indicates the current impossibility for first principles or semiempirical computations of χ_{eff} with enough accuracy to be of any practical value. Typical magnitudes of χ_{eff} for compatible blends are of the order or less than 10^{-2}. Thus, by use of the FH relation[1]

$$\chi_{eff}^{FH} = z(\epsilon_{11} + \epsilon_{22} - 2\epsilon_{12})/(2k_BT) \tag{1.1}$$

between the appropriate Flory-Huggins theory effective interaction parameter χ_{eff}^{FH} and the individual van der Waals interaction energies ϵ_{ij}, $i, j = 1, 2$, the absolute temperature T, and the lattice coordination number z, it becomes clear that the difference between the van der Waals energies $\epsilon \equiv \epsilon_{11} + \epsilon_{22} - 2\epsilon_{12}$ is on the order or less than 1 cal/segment mol, a magnitude that therefore it not amenable to computation by the most sophisticated quantum mechanical or molecular mechanics methods presently available. Consequently, it appears more useful to establish general trends concerning how χ_{eff} varies with monomer structure and interactions to assist in the design of new materials.

FH theory, however, provides no clue as to the relation beween χ_{eff} and microscopic molecular structure other than the obvious suggestion that chemical donor-acceptor type interactions should make χ_{eff} more negative and thereby favor blend compatibility. This lack of a molecular understanding for χ_{eff} is but one of the many limitations to the otherwise immensely useful FH theory. Other limitations to the theory stem from the contradictions of its predictions with experimental observations as follows: FH theory in eq 1.1 predicts χ_{eff} to be inversely proportional to the absolute temperature and to be independent of composition, molecular weights, and pressure. However,

0024-9297/91/2224-5096$02.50/0

experimental determinations show χ_{eff} generally to have a considerable temperature-independent contribution. The latter is often called "the entropic part of the interaction energy" despite the obvious internal contradiction. Furthermore, experiments find a rich composition and molecular weight dependence of χ_{eff}. Thus, composite properties might be considerably altered by exploiting this composition, temperature, molecular weight, etc., variation of χ_{eff} whose molecular origins had remained an enigma for almost 50 years.

The above noted strong contradictions between FH theory and experiments imply either that the lattice model, upon which the theory is originally formulated, is deficient, that the approximations, used in deriving the theory from the lattice model, are inadequate, or both. The standard lattice model is defined as having the polymer chains formed by sequentially placing monomers at the sites of a regular lattice, restricting site occupancy to a single monomer or solvent molecule, and including nearest-neighbor van der Waals interactions. It is clear that the lattice represents an over simplification,[2] but Sanchez and co-workers[3] have shown how Flory–Huggins theory can be derived without use of an underlying lattice. Nevertheless, once improvements are made in the Flory–Huggins approximations to the lattice model, any deficiencies of the lattice model must emerge when comparisons are made between theory and experiment. Foremost among these limitations is the idealization of lattice models in requiring that the same single lattice site house one and only one monomer of any species in the system, despite the generally significant disparities in sizes and shapes of the different monomers.

It is, therefore, desirable to incorporate monomer sizes and shapes realistically into the lattice model[4] in order to provide a more molecular basis for understanding the properties of blends. As an illustration, Figure 1 provides some examples of polymers with structured monomers on the simplest cubic lattice. Unfortunately for our knowledge, FH theory is completely unable to describe the variation of polymer properties with the different schematic chain structures in Figure 1 because the approximations inherent in FH theory ignore all the short-range correlations that are necessary to distinguish between these monomer structures.[5] Thus, the accompanying paper and some of our earlier works are devoted to generalizing the standard lattice model of polymers so that it includes monomer structural details,[4,6] such as those in Figure 1, and to developing methods for systematically calculating the corrections[4-9] to FH theory because these corrections enable determination of relationships between monomer (and solvent molecule) structure and the physical properties of melts, blends, and concentrated polymer solutions.

Other deficiencies of Flory–Huggins theory have also been apparent for a long time. Indeed, Flory developed equation of state theories[10] to rectify some of these perceived problems, but again these theories are replete with phenomenological parameters that currently cannot be related quantitatively to monomer structures and monomer microscopic interactions, a limitation in common with FH theory. The equation of state theories are primarily designed to model the equations of state of pure substances and mixtures, and they provide important information concerning central theoretical elements that must be appended to the standard lattice model of polymer systems.[11] First of all, polymer melts, blends, and concentrated solutions are compressible systems whose properties cannot adequately be described by the widely used incompressible FH theory. Equation of state theories

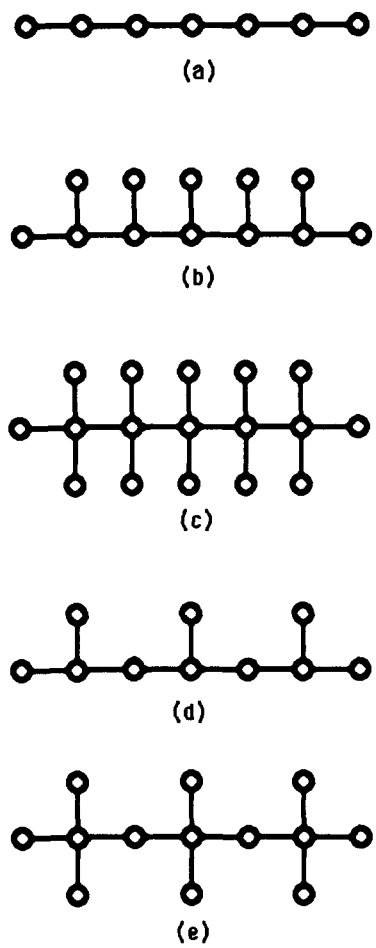

Figure 1. Examples of polymer chains with $N = 6$ backbone bonds and different monomer structures, drawn for simplicity stretched out in two dimensions. All junctions in the polymer chains *a–e* are fully flexible. The architecture *a* represents a linear chain with the site occupancy index $M = N + 1$, while the structures *b–e* depict branched chains with the ratio $M/N > 1$.

indicate how this compressibility strongly affects thermodynamic properties through the so-called equation of state terms. Thus, it is clear that compressibility must be incorporated into a theory in order to pose the interesting and practically important question as to whether pressure dependences may be used to modify the properties and performance of composite materials. Our previous paper illustrates how blend compressibility affects the molecular interpretation[12] of small-angle neutron scattering interaction parameters χ_{eff}. Hence, we find that it is necessary for any generalization of the lattice model to account for the compressibility of these polymeric liquids in order to properly describe the thermodynamics of these systems before any attempt is made to relate monomer structure to the properties of composites.

Here we apply the general lattice cluster theory predictions of the preceding paper[13] to study the influence of monomer structure and compressibility (and hence pressure) on the properties of polymer blends. The examples in Figure 1 are adequate for determining which blend properties are sensitive to monomer structure, and paper 3 on comparison with experimental data for PS/PVME blends studies this point further through a consideration of a large number of vinyl monomer structures. The particular properties treated are the extrapolated zero-angle neutron scattering experiment definitions of an effective χ_{eff} parameter and the excess thermodynamic properties ΔS^{mix}, ΔH^{mix}, and ΔV^{mix}. Other thermodynamic properties may readily be evaluated from the free energy

expressions we provide here. Prior thermodynamic models of polymer blends have extensively studied excess thermodynamic properties, so the majority of our illustrations involve the neutron scattering χ_{eff}, whose dependence on pressure has to our knowledge not been investigated previously.

Section II briefly introduces the lattice model, some notation, and a convenient specialization of the results of paper 1 to binary blends.[13] This section is designed for those desiring only a brief introduction to the theory and not the lengthy presentation of the preceding paper. Those more interested in results may skip to section III, where various definitions of the effective interaction parameter χ_{eff} are provided along with illustrations of how this χ_{eff} varies with composition, monomer structure, pressure, van der Waals interaction energies, and molecular weights. Several general trends are established, and a wide variety of shapes are obtained for curves of χ_{eff} versus composition. We show how an apparently athermal χ_{eff} may arise in a compressible system with considerable attractive interactions and a nonzero χ_{eff}^{FH} provided molecular weights are not too high. The temperature dependence of χ_{eff} will be discussed more thoroughly in the following paper on PS/PVME blends. It turns out that the neutron scattering χ_{eff} parameter displays the greatest qualitative sensitivity to monomer structures, and this gives another motivation for our emphasis on this particular property of blends. The excess thermodynamic quantities are also provided as a function of composition, monomer structure, pressure, van der Waals interaction energies, and molecular weights. The calculations here consider low molecular weights to emphasize molecular weight dependences as a vehicle to aid in experimentally determining the microscopic interaction energies. Paper 4 of this series will study the limiting high molecular weight χ_{eff}.

The dependence of excess thermodynamic quantities on monomer structures is more a quantitative rather than qualitative matter, and different measures of an effective interaction parameter χ_{eff} are shown often to provide disparate values. Thus, the latter feature suggests the need for caution in blindly substituting experimental χ_{eff} into theories of polymer properties when the actual χ_{eff} is composition dependent and is influenced by compressibility. An example of the types of errors incurred will be presented elsewhere in a study of interfacial profiles in phase-separated blends.[14] Section IV describes a comparison of our computed neutron scattering effective interaction parameter χ_{eff} with those obtained from continuum RISM theory calculations. Many general qualitative trends are found to be identical in both approaches, stressing their complementary nature. The preceding paper also discusses comparisons with phenomenological models such as van der Waals fluid models.

II. Lattice Model and Cluster Expansion for Packing Entropies

The standard lattice model of binary compressible polymer blends places the unit polymer segments (monomers) at the sites of a regular array of N_l sites and coordination number z. A set of n_v sites remains vacant and represents the excess (or liquidlike) free volume in the system. The volume fraction $\phi_v = n_v/N_l$ of this free volume may be specified in terms of the equation of state by fixing the system's pressure. The two polymer components are assumed to be monodisperse, and chains of species 1 and 2, respectively, have $N_1 - 1$ and $N_2 - 1$ backbone bonds. All junctions are taken to be completely flexible. Excluded volume constraints apply to all the $N_l - n_v$ occupied lattice sites, prohibiting multiple occupancy. Attractive interactions are modeled by the nearest-neighbor van der Waals attractive energies ϵ_{11}, ϵ_{22}, and ϵ_{12} between the i–j species monomer pairs on neighboring sites.

Nemirovsky et al.[4] have generalized this standard lattice model such that individual monomers have detailed structures. Hence, each monomer occupies several lattice sites, where the submonomer units on different lattice sites are connected by flexible bonds as depicted in Figure 1. Such a generalization more faithfully represents the actual molecular structure. However, simple approximations to the lattice model, such as the classic FH approximation, do not distinguish between the different chain architectures like those depicted in Figure 1. Consequently, this generalized model is useful provided that sufficient corrections[4-6,8,9] are affixed to the FH mean field approximation.[1] These corrections may be evaluated by using the cluster expansion methods described in the preceding paper.[13] A briefer more pedagogical introduction to the methods is sketched below for those who do not wish to plow through the details of paper 1. For simplicity, the perturbative character of the lattice cluster theory (LCT) is illustrated here in terms of a one-component system of linear chain polymers, but the final expressions are quoted in a general form that is applicable to a compressible binary blend with arbitrary monomer structures. A given chain architecture may be represented by a linear sequence or a complicated branching pattern in which the monomers have specified structures. For the same reason as mentioned above, all chains of a given architecture have the same bonding topology and do not have small closed loops. Treating irregular structured chains can, however, be accomplished by specifying some additional counting indexes, described below.

The new algebraic derivation of the LCT employs rather simple mathematical methods and enables several computational advances to be made. Its advantages over the previous field theory formulation are described in our recent papers.[5,6,13]

A. Analytic Representation of Lattice Model. Two lattice sites i and j are nearest neighbors when their positions $\mathbf{r}_i$ and $\mathbf{r}_j$ (with respect to the origin of coordinates) satisfy the relation

$$\mathbf{r}_i = \mathbf{r}_j + \mathbf{a}_\beta \tag{2.1}$$

where $\mathbf{a}_\beta$, $\beta = 1, ..., z$ denote the vectors from a given lattice site to one of the z nearest-neighbor lattice sites. The nearest-neighbor condition 2.1 may be represented as a constraint condition by using a Kronecker δ as

$$\delta(\mathbf{r}_i,\mathbf{r}_j+\mathbf{a}_\beta) \equiv \delta(i,j+\beta) \tag{2.2}$$

where the right-hand side is a convenient shorthand notation that is used below to represent the bonding constraints. The system under consideration contains a set of n_p monodisperse linear polymers with $N - 1$ bonds each. The connectivity and possible orientations of the first bond on the first chain contributes to the packing partition function a factor of $\sum_{i_1{}^1,i_2{}^1}\sum_{\beta_1}\delta(i_1{}^1,i_2{}^1+\beta_1{}^1)$, where the subscript labels the sequential monomer number along the chain and the superscript labels the chain number. The next bond in this chain contributes to the partition function a factor of $\sum_{i_3{}^1}\sum_{\beta_2{}^1}\delta(i_2{}^1,i_3{}^1+\beta_2{}^1)$ with the obvious excluded volume constraint $i_3{}^1 \neq i_1{}^1$ between the nonbonded first and third monomers. This process is continued for all bonds and all chains. A factor of $(n_p!)^{-1}$ must be introduced to account for chain indistinguishability, and the equivalence of both chain ends requires

the symmetry number 2^{n_p}. Thus, the configurational partition function $W(n_p,N)$ for packing such n_p monodisperse linear polymers with polymerization indexes N can be written as

$$W(n_p,N) = \frac{1}{n_p!2^{n_p}} \times \sum_{\substack{i_1^1 \neq i_2^1 \neq \ldots \neq i_N^1 \\ \neq i_1^2 \neq i_2^2 \neq \ldots \neq i_N^2 \\ \ldots \\ \neq i_1^{n_p} \neq i_2^{n_p} \neq \ldots \neq i_N^{n_p}}} \prod_{m=1}^{n_p}\{\prod_{\alpha=1}^{N-1}\sum_{\beta_\alpha^m}^{z}\delta(i_\alpha^m,i_{\alpha+1}^m+\beta_\alpha^m)\} \quad (2.3)$$

The excluded volume constraint $i_\alpha^m \neq i_{\alpha+1}^m$ between successively bonded monomers on a single chain is inserted into (2.3) only for notational symmetry as the Kronecker δ functions in (2.3) already prohibit bonded monomers from occupying the same lattice site.

B. Exact Formal Solution and Flory–Huggins Approximation. In order to extract the approximate FH mean field contribution from (2.3) and to derive systematic rules for computing corrections to FH approximation, we first replace each Kronecker δ in (2.3) by its lattice Fourier transform

$$\delta(i,j+\beta) = N_l^{-1}\sum_{\mathbf{q}}\exp[i\mathbf{q}\cdot(\mathbf{r}_i - \mathbf{r}_j - \mathbf{a}_\beta)] \quad (2.4)$$

where N_l is the total number of lattice sites and the summation runs over the first Brillouin zone. Each Kronecker δ in (2.3) introduces through (2.4) the wave vector summation index $\mathbf{q}_\alpha^m$ for each bond. Separation of the $\mathbf{q} = 0$ terms in the sum of $\delta(i,j+\beta)$ in (2.4) over all directions $\beta = 1, \ldots, z$ leads to

$$\sum_\beta \delta(i,j+\beta) = \frac{z}{N_l}\left\{1 + \frac{1}{z}\sum_{\mathbf{q}\neq 0} f(\mathbf{q})\exp[i\mathbf{q}\cdot(\mathbf{r}_i - \mathbf{r}_j)]\right\} \quad (2.5)$$

where $f(\mathbf{q})$ is the nearest-neighbor structure factor

$$f(\mathbf{q}) = \sum_{\beta=1}^{z}\exp(-i\mathbf{q}\cdot\mathbf{a}_\beta) \quad (2.6)$$

and finally to another *exact* algebraic representation of the packing partition function (2.2) as

$$W(n_p,N) = \frac{1}{n_p!2^{n_p}}\sum_{i_1^1 \neq \ldots \neq i_N^{n_p}}\prod_{m=1}^{n_p}\prod_{\alpha=1}^{N-1}\left[\frac{z}{N_l}\right] \times \left\{1 + \frac{1}{z}\sum_{\mathbf{q}_\alpha^m \neq 0} f(\mathbf{q}_\alpha^m)\exp[i\mathbf{q}_\alpha^m\cdot(\mathbf{r}_{i^m_\alpha} - \mathbf{r}_{i^m_{\alpha+1}})]\right\} \quad (2.7)$$

The product over indexes α, m in (2.7) is written more compactly as

$$W(n_p,N) = \frac{1}{n_p!2^{n_p}}\sum_{i_1^1 \neq \ldots \neq i_N^{n_p}}\prod_{m=1}^{n_p}\prod_{\alpha=1}^{N-1}\left\{\left[\frac{z}{N_l}\right][1 + X_{\alpha,m}]\right\} \quad (2.8)$$

where the terms $X_{\alpha,m}$ are defined for each polymer bond α, m by

$$X_{\alpha,m} = \frac{1}{z}\sum_{\mathbf{q}_\alpha^m \neq 0} f(\mathbf{q}_\alpha^m)\exp[i\mathbf{q}_\alpha^m\cdot(\mathbf{r}_{i^m_\alpha} - \mathbf{r}_{i^m_{\alpha+1}})] \quad (2.9a)$$

and describe the influence of correlations on the possible ways of packing the set of flexible chains on the lattice. The expansion of the product over polymer bonds, i.e., over α and m, in (2.8) produces a cluster expansion similar in spirit to the expansion derived before the inception of FH theory by Mayer[15] to compute the virial coefficients for a nonideal gas.

The leading contribution in (2.8) arises from the factor of unity for each α–m pair and yields the mean field approximation

$$W^{MF}(n_p,N) = \frac{1}{n_p!2^{n_p}}\sum_{i_1^1 \neq \ldots \neq i_N^{n_p}}\prod_{m=1}^{n_p}\prod_{\alpha=1}^{N-1}\left[\frac{z}{N_l}\right] \quad (2.9b)$$

Since the summand in (2.9) does not depend on monomer positions, the summations are easily performed to give

$$W^{MF}(n_p,N) = \frac{1}{n_p!2^{n_p}}\frac{N_l!}{(N_l - n_pN)!}\left[\frac{z}{N_l}\right]^{n_p(N-1)} \quad (2.10)$$

which recovers the classic Flory–Huggins combinatorial packing entropy of mixing[1] for the set of n_p polymers, while its generalization to blends provides the corresponding FH entropy for this system (with immediate self-reversals included).[7] The remaining terms from the cluster expansion in (2.8), therefore, produce corrections to the FH approximation as arising from correlations, neglected entirely by Flory, between the placement of different monomers and bonds on the lattice.

C. Cluster Expansion for Packing Entropies. The quantities $X_{\alpha,m}$ in (2.8) depend on the explicit positions of the two segments forming the αth bond on the mth polymer chain, and thus the $X_{\alpha,m}$ represent the corrections arising from correlations in monomer positions. Expanding the product in (2.8) provides the cluster expansion form

$$1 + \sum_{\alpha,m}X_{\alpha,m} + \sum_{\alpha,m>\alpha',m'}X_{\alpha,m}X_{\alpha',m'} + \ldots \quad (2.11)$$

where the designation $\alpha,m > \alpha',m'$ indicates that the summation in (2.10) runs over all *distinct* pairs of bonds. The linear terms in $X_{\alpha,m}$ are called the one-bond contributions, the quadratic are the two-bond contributions, etc. When substituted into (2.7), the leading term of unity in (2.11) generates the leading FH approximation of (2.10), while the remainder of (2.11) produces, respectively, the correlated one-bond, two-bond, etc., contributions to the cluster expansion. The summation over distinct lattice sites in (2.7) runs over those lattice sites connected by the correlating bonds, as indicated in the summation indexes of (2.11), along with the remaining lattice sites that are either unoccupied or have uncorrelated monomers. Previous papers describe the evaluation of individual terms in the expansion (2.11),[4,6,8,9] the use of Mayer-like diagrams to represent various contributions to this cluster expansion,[5,6,13] the treatment of the van der Waals interaction energies,[5,6,9,13] and the methods for generalizing the theory to multicomponent systems with structured monomers.[5,6,13] Thus, we omit these details here.

D. Results for Compressible Binary Blends. In order to conform to the notation[13] of paper 1 for describing structured monomers, the chains are now taken to have N_i bonds along the chain backbone and to cover M_i lattice sites per chain. The structure dependence in the blend free energy expressions of Table I enters through the combinatorial numbers $N_i^{(l)}$ that describe the architecture of species l. Values of the $N_i^{(l)}$ for polymers with the structures a–c in Figure 1 are presented in Table I of Nemirovsky et al.,[4] while generalization to other architectures emerges from the following definitions: $N_i^{(l)}$ is the number of sequential sets of i bonds in a polymer that covers M sites; $N_{i,j}^{(l)}$ is the number of nonsequential sets of i and j bonds, $N_\perp^{(l)}$ is the number of ways in which three bonds

Table I
Helmholtz Free Energy of a Compressible Binary Blend ($\phi_1 + \phi_2 + \phi_v = 1$)[a]

$$\frac{F}{N_l k_B T} = \phi_v \ln \phi_v + \frac{\phi_1}{M_1} \ln \phi_1 + \frac{\phi_2}{M_2} \ln \phi_2 + \phi_1\phi_2 \sum_{\substack{i=0 \\ i+j\le 4}}^{4}\sum_{j=0}^{4} g_{12}^{(i,j)} \phi_1^{\,i} \phi_v^{\,j} + \sum_{k=1}^{2} \phi_k \phi_v \sum_{\substack{i=0 \\ i+2j\le 6}}^{2}\sum_{j=0}^{3} g_{kv}^{(i,j)} \phi_k^{\,i} \phi_v^{\,j} + f_1\phi_1 + f_2\phi_2$$

$$g_{12}^{(a,b)} = \frac{1}{z} A_0^{(a,b)} + \frac{1}{z^2} \sum_i A_i^{(a,b)} + \sum_i B_i^{(a,b)} + \sum_i C_i^{(a,b)}$$

$$A_0^{(0,0)} = \Delta_1^{\,2}$$

$$A_1^{(0,0)} = \Delta_2^{\,2} + 4N(1,2)\Delta_1^{\,2}[2N(1,1) + N(1,2) + 2] + 4\Delta_1\left[-\frac{1}{2}\Delta_A + \frac{2}{3}\Delta_1^{\,2} + \frac{1}{2}\Delta_1^{\,3} + 2N(1,2)\Delta_{1,1} + \Delta_1 K(1,1;1)\right]$$

$$B_1^{(0,0)} = \epsilon\left[\frac{z}{2} - N(1,1)\right] + \frac{\epsilon}{z}\{R(1) - 2N(1,2)[N(1,1) + 2N(2,1) + 2K(1,1;1)]\}$$

$$C_1^{(0,0)} = -\epsilon^2\left[\frac{1}{2}N(1,1) + N(2,1) + K(1,1;1)\right]$$

$$A_0^{(1,0)} = 0$$

$$A_1^{(1,0)} = 2\Delta_1^{\,2}\left[\frac{4}{3}\Delta_1 + 4N(1,2)\Delta_1 + \Delta_1^{\,2} + 2\Delta_{1,1}\right]$$

$$B_1^{(1,0)} = \epsilon\Delta_1 - \frac{\epsilon}{z}\Delta_A - 4\frac{\epsilon}{z}[[1 + N(1,2)]\Delta_1^{\,2} + K(1,1;1)\Delta_1 - N(1,2)\Delta_{1,1} + N(2,1)\Delta_1 - N(1,1)\Delta_2]$$

$$C_1^{(1,0)} = \epsilon^2\left[-\frac{z}{4} + \frac{1}{2}\Delta_1 + 2N(1,1) + 2N(2,1) - [N(1,1)]^2 + 3K(1,1;1)\right]$$

$$A_0^{(2,0)} = 0$$

$$A_1^{(2,0)} = 2\Delta_1^{\,4}$$

$$B_2^{(2,0)} = 4\frac{\epsilon}{z}\Delta_1[\Delta_1 + \Delta_{1,1} + N(1,2)\Delta_1 - \Delta_1^{\,2}]$$

$$C_1^{(2,0)} = \epsilon^2\left[\frac{z}{4} - 2\Delta_1 - 2N(1,1) - N(2,1) - N(2,2) - 3K(1,1;1) + 3\Delta_1^{\,2} + 2[N(1,1)]^2 - [N(1,2)]^2\right]$$

$$A_i^{(3,0)} = 0$$

$$B_1^{(3,0)} = 4\frac{\epsilon}{z}\Delta_1^{\,3}$$

$$C_1^{(3,0)} = \epsilon^2[2\Delta_1 + \Delta_{1,1} - 6\Delta_1^{\,2} - [N(1,1)]^2 + [N(1,2)]^2]$$

$$A_0^{(0,1)} = 0$$

$$A_1^{(0,1)} = 4N(1,2)[N(1,2)\Delta_{1,1} + 2N(1,1)K(1,1;2)]$$

$$A_2^{(0,1)} = 2[N(1,2)]^2\left[4N(1,1) - \frac{4}{3}N(1,2) + 8N(1,1)N(1,2) - 3[N(1,2)]^2\right]$$

$$B_1^{(0,1)} = -\epsilon N(1,2) + \frac{\epsilon}{z}R(2) + \epsilon_\Delta\left[-\Delta_1 + \frac{1}{z}\Delta_A\right]$$

$$B_2^{(0,1)} = \frac{2}{z}[\epsilon - \epsilon_\Delta]\{2N(1,2)[\Delta_1 + N(1,2)\Delta_1 + \Delta_{1,1}] + [N(1,2)N(2,1) - N(1,1)N(2,2)]\}$$

$$C_1^{(0,1)} = \frac{1}{8}[\epsilon - \epsilon_\Delta]^2[-z + 6\Delta_1 + 4N(1,2) + 6N(2,1) + 8K(1,1;1)] - \frac{1}{2}\epsilon_\Delta^{\,2}[N(1,1) + 2N(2,1) + 2K(1,1;1)]$$

$$A_0^{(0,2)} = 0$$

$$A_2^{(0,2)} = -2[N(1,2)]^3[4N(1,1) - N(1,2)]$$

$$B_1^{(0,2)} = \frac{4}{z}[\epsilon - \epsilon_\Delta]N(1,2)[N(1,2) + K(1,1;2) - N(1,2)\Delta_1 + [N(1,2)]^2]$$

$$B_2^{(0,2)} = -\frac{4}{z}\epsilon_{22}\{N(1,1)N(1,2)[3N(1,2) + 2] + N(1,2)K(1,1;1) + N(1,1)K(1,1;2)\}$$

$$C_1^{(0,2)} = \epsilon_{22}[\epsilon - \epsilon_{11}]\frac{z}{2} - 2\epsilon_{22}[\epsilon - \epsilon_\Delta]N(1,1) - 2\epsilon_{22}^{\,2}N(1,2)$$

$$C_2^{(0,2)} = -[\epsilon\epsilon_{22} + \epsilon_{11}\epsilon_\Delta]N(2,1) - [2\epsilon\epsilon_{22} + \epsilon_\Delta^{\,2}]K(1,1;1)$$

$$C_3^{(0,2)} = \frac{1}{4}[-\epsilon^2 + 2\epsilon[\epsilon_{11} - 3\epsilon_{22}] - \epsilon_\Delta^{\,2} + 4\epsilon_\Delta\epsilon_{22}][N(2,2) + 2N(1,2)[\Delta_1 - 1]]$$

$$A_i^{(0,3)} = 0$$

$$B_1^{(0,3)} = -\frac{4}{z}[\epsilon - \epsilon_\Delta][N(1,2)]^3 + 12\epsilon_{22}N(1,1)[N(1,2)]^2$$

$$C_1^{(0,3)} = 2\epsilon_{22}[\epsilon_{22}N(1,1) - 2[\epsilon - \epsilon_{11}]N(1,2) + 2[\epsilon - \epsilon_\Delta + \epsilon_{22}]N(1,1)N(1,2)]$$

$$C_2^{(0,3)} = -\epsilon_\Delta[\epsilon_{11} + \epsilon_{22}]K(1,1;1) - 2\epsilon_{22}[\epsilon - \epsilon_\Delta]K(1,1;2)$$

$$C_3^{(0,3)} = \frac{1}{2}[-\epsilon^2 + 2\epsilon[\epsilon_{11} - 9\epsilon_{22}] - \epsilon_\Delta^{\,2} + 2\epsilon_{22}[8\epsilon_{11} - 5\epsilon_{22}]][N(1,2)]^2$$

Table I (Continued)

$$\frac{F}{N_l k_B T} = \phi_v \ln \phi_v + \frac{\phi_1}{M_1} \ln \phi_1 + \frac{\phi_2}{M_2} \ln \phi_2 + \phi_1\phi_2 \sum_{\substack{i=0 \\ i+j\le 4}}^{4}\sum_{j=0}^{4} g_{12}^{(i,j)} \phi_1^{\,i} \phi_v^{\,j} + \sum_{k=1}^{2} \phi_k \phi_v \sum_{\substack{i=0 \\ i+2j\le 6}}^{2}\sum_{j=0}^{3} g_{kv}^{(i,j)} \phi_k^{\,i} \phi_v^{\,j} + f_1\phi_1 + f_2\phi_2$$

$$A_0^{(1,1)} = 0$$

$$A_1^{(1,1)} = 4[N(1,2)]^2[[N(1,1)]^2 - [N(1,2)]^2 + 2\Delta_1^{\,2}]$$

$$B_1^{(1,1)} = -\frac{4}{z}\{\epsilon_\Delta \Delta_1[\Delta_1 + \Delta_{1,1} + 2N(1,2)\Delta_1] + \epsilon[N(1,2)\Delta_{1,1} + K(1,1;2)\Delta_1] - 2\epsilon[\Delta_1 - N(1,2) - 1]N(1,2)\Delta_1\}$$

$$C_1^{(1,1)} = [\epsilon^2 - 2\epsilon\epsilon_\Delta]\frac{z}{4} + \frac{1}{2}[-5\epsilon^2 + 10\epsilon\epsilon_\Delta - \epsilon_\Delta^{\,2}]\Delta_1 + 2\epsilon\epsilon_\Delta N(1,2)$$

$$C_2^{(1,1)} = \frac{1}{4}[-3\epsilon^2 + 6\epsilon\epsilon_\Delta + \epsilon_\Delta^{\,2}]\Delta_2 - [2\epsilon^2 - 3\epsilon\epsilon_\Delta]N(2,2)$$

$$C_3^{(1,1)} = \frac{1}{2}[5\epsilon^2 - 6\epsilon\epsilon_\Delta + \epsilon_\Delta^{\,2}]\Delta_1^{\,2} - \epsilon^2[N(1,1)]^2 - 2[\epsilon^2 - 2\epsilon\epsilon_\Delta]K(1,1;1)$$

$$A_i^{(2,1)} = 0$$

$$B_1^{(2,1)} = -\frac{4}{z}\epsilon_\Delta \Delta_1^{\,3} - \frac{12}{z}\epsilon N(1,2)\Delta_1^{\,2}$$

$$C_1^{(2,1)} = \epsilon^2[2\Delta_1 + \Delta_{1,1} - 2N(1,2) - K(1,1;2)] - 2\epsilon\epsilon_\Delta[2\Delta_1 + \Delta_{1,1}]$$

$$C_2^{(2,1)} = \frac{1}{2}[-17\epsilon^2 + 18\epsilon\epsilon_\Delta - \epsilon_\Delta^{\,2}]\Delta_1^{\,2} + 2\epsilon^2[2[N(1,1)]^2 - [N(1,2)]^2]$$

$$A_i^{(1,2)} = 0$$

$$B_1^{(1,2)} = \frac{4}{z}\{[3\epsilon[N(1,2)]^2\Delta_1 - \epsilon_\Delta[N(1,2)]^2[2\Delta_1 + N(1,1)]] - 3\epsilon_{22}N(1,1)N(1,2)\Delta_1\}$$

$$C_1^{(1,2)} = 2\epsilon_{22}[2\epsilon - 2\epsilon_{11} + \epsilon_{22}]\Delta_1 - 2[\epsilon^2 - 2\epsilon\epsilon_\Delta + \epsilon_\Delta[\epsilon_1 + \epsilon_{22}]]N(1,2)$$

$$C_2^{(1,2)} = -[4\epsilon\epsilon_{22} + \epsilon_\Delta[\epsilon_{11} - 3\epsilon_{22}]]\Delta_1^{\,2} - \epsilon^2[N(1,2)]^2 - [\epsilon^2 - 2\epsilon\epsilon_\Delta]K(1,1;2)$$

$$C_3^{(1,2)} = [5\epsilon^2 - 2\epsilon[5\epsilon_{11} - 7\epsilon_{22}] + 3\epsilon_\Delta^{\,2}]N(1,2)\Delta_1 + [2\epsilon\epsilon_{22} + \epsilon_\Delta^{\,2}]\Delta_{11}$$

$$A_i^{(2,2)} = B_i^{(2,2)} = 0$$

$$C_1^{(2,2)} = 3[[2\epsilon\epsilon_{22} + \epsilon_\Delta^{\,2}]\Delta_1^{\,2} + [3\epsilon_2 - 4\epsilon\epsilon_\Delta][N(1,2)]^2 - 2[\epsilon^2 - 2\epsilon\epsilon_\Delta]N(1,1)N(1,2)]$$

$$A_i^{(3,1)} = B_i^{(3,1)} = 0$$

$$C_1^{(3,1)} = 3\epsilon^2[\Delta^{12} - 2N(1,2)\Delta_1] - 6\epsilon\epsilon_\Delta\Delta_1^{\,2}$$

$$A_i^{(1,3)} = B_i^{(1,3)} = 0$$

$$C_1^{(1,3)} = 3\{\epsilon_{22}^{\,2}[N(1,1)]^2 - 4\epsilon_{22}[\epsilon - \epsilon_\Delta]N(1,1)N(1,2) + [\epsilon^2 - 2\epsilon[\epsilon_{11} - 3\epsilon_{22}] - 2\epsilon_\Delta^{\,2} - \epsilon_{11}^{\,2}][N(1,2)]^2\}$$

$$A_i^{(4,0)} = B_i^{(4,0)} = 0$$

$$C_1^{(4,0)} = 3\epsilon^2\Delta_1^{\,2}$$

$$A_i^{(0,4)} = B_i^{(0,4)} = 0$$

$$C_1^{(0,4)} = 3\epsilon_{22}[2\epsilon - 2\epsilon_{11} + \epsilon_{22}][N(1,2)]^2 - 6\epsilon_{22}^{\,2}N(1,1)N(1,2)$$

$$g_{\alpha v}^{(0,0)} = \frac{1}{z}[N(1,\alpha)]^2 + \frac{1}{z^2}\left\{-2N(1,\alpha)R(\alpha) + [N(2,\alpha)]^2 + 2[N(1,\alpha)]^2\left[\frac{4}{3}N(1,\alpha) + [N(1,\alpha)]^2 + 2K(1,1;\alpha)\right]\right\} + \epsilon_{\alpha\alpha}\frac{z}{2}$$

$$g_{\alpha v}^{(1,0)} = \frac{2}{z^2}[N(1,\alpha)]^2\left[\frac{4}{3}N(1,\alpha) + [N(1,\alpha)]^2 + 2K(1,1;\alpha)\right]$$

$$g_{\alpha v}^{(2,0)} = \frac{2}{z^2}[N(1,\alpha)]^4$$

$$g_{\alpha v}^{(0,1)} = -\epsilon_{\alpha\alpha}N(1,\alpha) + \frac{\epsilon_{\alpha\alpha}}{z}R(\alpha) - \frac{1}{2}\epsilon_{\alpha\alpha}^{\,2}N(1,\alpha)$$

$$g_{\alpha v}^{(1,1)} = -\frac{4}{z}\epsilon_{\alpha\alpha}N(1,\alpha)[N(1,\alpha) + K(1,1;\alpha)] - \epsilon_{\alpha\alpha}^{\,2}\left[\frac{z}{4} - 2N(1,\alpha)\right]$$

$$g_{\alpha v}^{(1,2)} = -\frac{4}{z}\epsilon_{\alpha\alpha}[N(1,\alpha)]^3 - 2\epsilon_{\alpha\alpha}^{\,2}N(1,\alpha)$$

$$g_{\alpha v}^{(0,2)} = -\epsilon_{\alpha\alpha}^{\,2}N(2,\alpha)$$

$$g_{\alpha v}^{(1,2)} = -\epsilon_{\alpha\alpha}^{\,2}[N(1,\alpha)]^2$$

$$g_{\alpha v}^{(2,2)} = 3\epsilon_{\alpha\alpha}^{\,2}[N(1,\alpha)]^2$$

$$g_{\alpha v}^{(0,3)} = -\epsilon_{\alpha\alpha}^{\,2}K(1,1;\alpha)$$

[a] $N(i,\alpha) \equiv N_i^{(\alpha)}/M_\alpha$, $\alpha = 1, 2$; $N(i,j;\alpha) \equiv N_{i,j}^{(\alpha)}/M_\alpha$, $\alpha = 1,2$; $K(i,j;\alpha) \equiv N(i,j;\alpha) - [1/2]^{\delta(i,j)}N(i,\alpha)N(j,\alpha)M_\alpha$, $\alpha = 1, 2$; $\delta(i,j) = 1$, $i = j$, $\delta(i,j) = 0$, otherwise, $\Delta_i \equiv N(i,1) - N(i,2)$, $\Delta_{i,j} \equiv K(i,j;1) - K(i,j;2)$, $R(\alpha) \equiv 2N(2,\alpha) + N(3,\alpha) + 3N(\perp,\alpha) + K(1,2;\alpha)$, $\alpha = 1, 2$; $\Delta_\Lambda \equiv 2\Delta_2 + \Delta_3 + 3\Delta_\perp + \Delta_{1,2}$, $\epsilon \equiv \epsilon_{11} + \epsilon_{22} - 2\epsilon_{12}$, $\epsilon_\Delta \equiv \epsilon_{11} - \epsilon_{22}$.

meet at a lattice site for a polymer chain, etc. (In contrast to paper 1, the definitions of $N_{i,i}^{(l)}$ in ref 4 do not include the symmetry number of 1/2!, which is, however, properly included in the calculated entropies in that paper.) These structure-specific combinatorial indexes are readily evaluated for polymers or solvent molecules with regular repeating or rather irregular architectures, and values of these counting indexes will be presented in a future paper for a wide variety of vinyl monomer structures.

Table I presents the free energy of mixing for a compressible structured monomer binary blend as formal expansion in the set of ϵ_{ij}/k_BT with the schematic form

$$\frac{\Delta F^{mix}}{N_l k_B T} = \frac{\phi_1}{M_1}\ln\phi_1 + \frac{\phi_2}{M_2}\ln\phi_2 + \phi_v \ln\phi_v + \sum_{i=1}^{\infty}\sum_{j,l=1,2} a_i^{(jl)}(\epsilon_{jj}/k_BT + \epsilon_{ll}/k_BT + \epsilon_{jl}/k_BT)^i \quad (2.12)$$

where $\phi_j = n_jM_j/N_l$ is the volume fraction of species j. The coefficients $a_i^{(jl)}$ are further expanded in a series of z^{-1}. All terms through order z^{-2} are retained in the order ϵ_{jl} contributions in Table I; those in ϵ_{jl}^2 contain the order z^{-1} corrections to the leading extended mean field (EMF) term; while only the leading EMF contributions of orders ϵ_{jl}^3 and ϵ_{jl}^4 are retained. The results in Table I are obtained from those in paper 1 by specializing to a binary blend and by extensive use of the relation $\phi_1 + \phi_2 = 1 - \phi_v$ to represent the noncombinatorial portion of the free energy as a linear superposition of the free energies of the individual pure melts (terms in the $g_{kv}^{(i,j)}$) plus a binary blend portion (terms in the $g_{12}^{(i,j)}$). The binary term displays a rather complicated and nonintuitive dependence on ϕ_v, arising from the fact that the presence of voids alters the nature of local corrections between interacting portions of the two different components. Since the voids make the system quasi-three-component, the form of Table I stresses the general lack of pairwise additivity of LCT predictions and contrasts them to the assumed pairwise additivity in phenomenological models.[16] Despite the apparent complexity of Table I, these expressions are rather simple as they involve a power series in the compositions with coefficients that depend on molecular weights, van der Waals energies, and monomer structure through the counting indexes $N_i^{(l)}$. Thus, these single expressions apply to polymer blends of *all compositions, molecular weights, monomer structures, temperatures,* and *free volume fractions* (equivalent to pressures after we transform to a constant-pressure system). This analytic simplicity and generality far outweights deficiencies inherent to any lattice model. Paper 1 provides a discussion of several possible improvements that may be introduced into the lattice model, but these are not considered further here because our primary goal is to illustrate the rich variety of behaviors that are predicted by the generalized LCT.

III. Flory Effective Interaction Parameter χ_{eff} for Compressible Binary Polymer Blends

This section specializes the theory to a compressible binary blend in which the two polymer species occupy M_1 and M_2 lattice sites and perhaps have different monomer structures. (M_i is the product of the polymerization index and the number of lattice sites per monomer of species i.) Once the effective interaction parameter χ_{eff} becomes composition dependent, the determination of χ_{eff} from measurements of different properties, such as small-angle neutron scattering, heats of mixing, solvent activities, etc., is generally known to produce different and unequal definitions of the χ_{eff} parameters. Our interest here lies in probing the combined influence of monomer structure and compressibility on these various χ_{eff} parameters. It turns out that by far the most sensitive to structure and compressibility is the χ_{eff} from small-angle neutron scattering measurements. Thus, this χ_{eff} is considered in most detail, but we also study how the heats of mixing and the volume change on mixing are affected by compressibility and monomer structures. The variations with compressibility are analyzed by computing pressure dependences of these thermodynamic quantities.

The effective site–site Flory interaction parameter χ_{eff} is traditionally[17] defined by neutron scattering experimentalists in terms of the extrapolated zero-angle coherent scattering function $S_{11}(0)^{-1}$ and the incompressible random-phase approximation (RPA)[18] as

$$\chi_{eff} = -\frac{1}{2}\left[S_{11}(0)^{-1} - \frac{1}{M_1\Phi_1} - \frac{1}{M_2\Phi_2}\right] \quad (3.1)$$

where the nominal volume fractions, $\Phi_i \equiv n_iM_i/(n_1M_1 + n_2M_2)$, $i = 1, 2$, are composition variables that satify the normalization condition

$$\Phi_1 + \Phi_2 = 1 \quad (3.2)$$

and, for simplicity, the scattering contrast is assumed to be complete. Equation 3.1 is a common empirical definition of χ_{eff}, and this is an important point which is discussed further below.

A slightly modified definition of χ_{eff} employs experimental volume fractions

$$\Phi_i^{(exp)} \equiv V_i/(V_1 + V_2) \quad (3.2a)$$

where V_i is the volume of the melt of pure i that is used in forming the blend. In this case, eq 3.1 is replaced by

$$\chi_{eff} = -\frac{1}{2}\left[S_{11}(0)^{-1} - \frac{1}{M_1\Phi_1^{(exp)}} - \frac{1}{M_2\Phi_2^{(exp)}}\right] \quad (3.3)$$

The differences between (3.1) and (3.3) are associated with the empirical method chosen for specifying volume fractions. Equations 3.1 and 3.3 refer the effective interaction to a single lattice site. Sometimes the reference unit cell volume v_0 appears in the equations used in the literature, but this notational complexity is unnecessary here. The condition 3.2 implies that the nominal volume fractions Φ_i are related to the ϕ_i used in Table I by

$$\Phi_i = \phi_i/(1 - \phi_v) \qquad i = 1, 2 \quad (3.4)$$

Hence, the composition variables Φ_i are independent of the excess free volume whose volume fraction is $\phi_v = n_v/N_l$.

For future reference, the case of $\phi_v = 0$ corresponds to an incompressible blend. The zero-angle partial structure factor $S_{11}(0)$ is then related to the chemical potential μ_1 by

$$S_{11}^{inc}(0)^{-1} = \frac{N_l}{M_1^2 k_B T}\left.\frac{\partial\mu_1}{\partial n_1}\right|_{T,V} \quad (3.5)$$

and the small-angle neutron scattering Flory effective interaction parameter χ_{eff}^{inc} is defined as

$$\chi_{eff}^{inc} = -\frac{1}{2}\left[S_{11}^{inc}(0)^{-1} - \frac{1}{M_1\phi_1} - \frac{1}{M_2\phi_2}\right] \quad (3.6)$$

with $\phi_1 + \phi_2 = 1$ only in the incompressible limit.

Generalizing to compressible blends leads to the thermodynamic relation

$$S_{11}(0)^{-1} = \frac{N_l}{M_1^2 k_B T} \left.\frac{\partial \mu_1}{\partial n_1}\right|_{T,V,\mu_2} \tag{3.7}$$

The constant volume V constraint in (3.5) and (3.7) implies a fixed number N_l of lattice sites. The derivative at constant μ_2 in (3.7) is more conveniently expressed in terms of derivatives $\partial\mu_i/\partial n_j, i,j = 1,2$, at constant chain numbers n_i for species i. (See ref 9.) Thus, eqs 3.1 and 3.7 permit the evaluation of χ_{eff} from the LCT free energies of Table I for comparison with experimental data.

A binary blend is a simple case of the k-component polymer mixture considered in sections III and IV of paper 1. Thus, the free energy is obtained from eqs 4.7–4.9 of paper 1 for $k = 2$ and is rearranged in Table I to separate the "interaction" portion involving $g_{12}^{(i,j)}$ from that of the pure melts (the $g_{kv}^{(i,j)}$ terms). The resulting expression derived from Table I for χ_{eff} is too lengthy to be presented separately, but it is a straightforward ratio of polynomials in the volume fractions ϕ_1 and ϕ_2, in the dimensionless nearest-neighbor attractive interaction energies ϵ_{11}/k_BT, ϵ_{22}/k_BT, and $\epsilon_{12}k_BT$, and in the inverse lattice coordination number $1/z$. (A simple cubic lattice has $z = 6$.) The coefficients in this expansion contain molecular weight ratios of the form $(a_iM_1 - b_i)/M_1$ and $(c_iM_2 - d_i)/M_2$, where a_i, b_i, c_i, and d_i are monomer structure dependent numbers. Given a choice of monomer architectures for the two polymer species, χ_{eff} becomes a function of composition Φ_i, free volume ϕ_v, temperature T, chain site occupancy indexes M_1 and M_2, and van der Waals attractive energies $\epsilon_{11}, \epsilon_{22}$, and ϵ_{12}. We may convert the Helmholtz free energy in Table I to the Gibbs free energy G by specifying the pressure P and by using the equation of state to determine ϕ_v as a function of P and other state variables. This is the procedure applied in the majority of the calculations presented below.

Thermodynamically meaningful computations for χ_{eff} are obtained for the one-phase region. Thus, it is necessary to check the stability of a single phase. A compressible blend at constant volume V has the stability conditions

$$f_{\phi_i\phi_i} > 0 \qquad i = 1, 2 \tag{3.8}$$

$$f_{\phi_1\phi_1}f_{\phi_2\phi_2} - f_{\phi_1\phi_2}f_{\phi_2\phi_1} > 0 \tag{3.9}$$

where

$$f_{\phi_i\phi_j} \equiv \left.\frac{\partial^2(F/N_l)}{\partial\phi_i\,\partial\phi_j}\right|_{V,T} \tag{3.10}$$

is the second derivative of the specific Helmholtz free energy with respect to the volume fractions ϕ_i and ϕ_j of (4.6) and (4.7–4.9) of paper[13] 1.

While neutron scattering experiments are performed for a constant scattering volume V, the experimental sample is often maintained at a constant pressure. In this case, the stability condition for the whole sample is

$$\left.\frac{\partial^2 G}{\partial\Phi_1^2}\right|_{P,T} > 0 \tag{3.11}$$

Inversion of the equation of state gives $\phi_v = \phi_v[n_1,n_2, n_v(n_1,n_2,P,T)]$. Hence eq 3.4 implies that G is a somewhat more complicated function of n_1, n_2, P, and T than is F in Table I. However, it is straightforward to evaluate the derivative in (3.11) numerically to check for blend stability.

We now illustrate the general types of behavior predicted for χ_{eff} by the lattice cluster theory as we vary monomer structure, molecular weights, microscopic interaction parameters, and state variables. The examples depicted in Figures 2–4, 6–9, and 11–16 involve a model compressible binary blend in which linear chains are blended with those having structure b of Figure 1. The site occupancy indexes M_1 and M_2 of these linear and branched polymer species in Figures 2, 3, 5–10, and 12–16 are taken to be equal, $M_1 = M_2 = 100$. These low values of M_i accentuate molecular weight dependences in χ_{eff}, while subsequent papers will consider the high molecular weight limit. A detailed comparison with experimental data for PS/PVME blends and a further discussion of the influence of monomer structure and compressibility on zero-angle neutron scattering data and thermodynamic properties of blends are provided in paper 3.

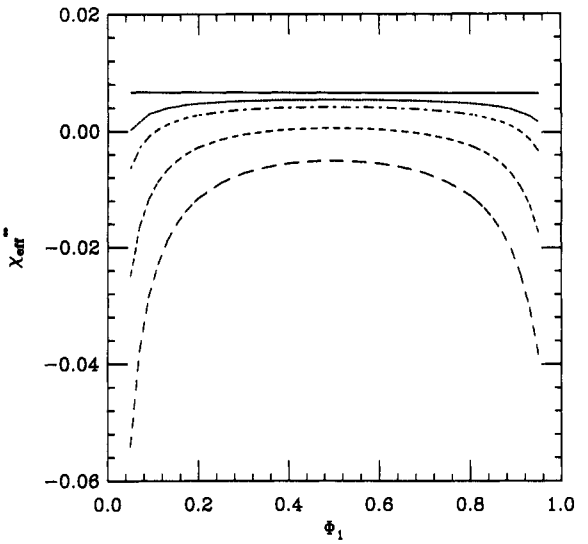

Figure 2. LCT idealized athermal limit small-angle neutron scattering effective interaction parameter $\chi_{eff}^{\infty}(\Phi_1)$ for various pressures: $P = 1000$ atm (– –), $P = 2000$ atm (- - -), $P = 4000$ atm (– · –), $P = 6000$ atm (···), and $P = \infty$ (i.e., incompressible limit) (—). The model binary blend is constructed from linear chains a and the branched ones b (see Figure 1) with the equal site occupancy indexes $M_1 = M_2 = 100$. The same model blend is employed through Figures 2–16. However, Figures 4 and 11 and 5 and 10 display, respectively, the behavior of χ_{eff}^{∞} (or χ_{eff}^{∞}) also for $M_1 = M_2 \neq 100$ or for blends composed of other monomer structure pairs of Figure 1. All figures have the composition variables Φ_1 (or Φ_1^{exp}) lie in the range 0.05–0.95, and unless otherwise specified the temperature is $T = 415.15$ K.

A. The Athermal Limit. Athermal polymer blends occupy a special place in the theory of polymer mixtures since their properties are presumed to be purely of entropic origin. An example is the PMMA/PEO blend studied by Russell and co-workers,[19] where the small-angle neutron scattering χ_{eff} appears to be temperature independent. Hence, the investigation of the athermal effective interaction parameter χ_{eff}^{∞} is designed to understand the molecular basis of this enigmatic "entropic interaction parameter". RISM calculations[20] consider this athermal blend by using a hard-sphere model without attractive interactions, and the natural lattice counterpart involves the case where all $\epsilon_{ij} = 0$. Therefore, we begin the description of LCT predictions with χ_{eff}^{∞} for athermal blends. Several examples are provided in Figures 2, 4, and 5. The influence of pressure P on χ_{eff}^{∞} is exhibited in Figure 2. The pressure P is evaluated from the Helmholz

free energy of Table I as

$$P = -\left.\frac{\partial F}{\partial V}\right|_{T,n_1,n_2} = -\frac{1}{a^3}\left.\frac{\partial F}{\partial n_v}\right|_{T,n_1,n_2} \quad (3.12)$$

where the lattice constant is a. This lattice constant and the temperature T are chosen as a = 2.5477 Å and T = 415.15 K in Figures 2–15. A more detailed study of the influence of monomer structure on temperature dependence of χ_{eff} will be presented in conjunction with our analysis of the PS/PVME system.

Because the excess free volume ϕ_v decreases with increasing P and varies only very slowly with composition at constant P, Figure 2 in effect also displays the general variation of χ^{∞}_{eff} with ϕ_v. An incompressible blend has no excess free volume (ϕ_v = 0), so χ^{∞}_{eff} must approach the incompressible limit at high P. In the high molecular weight limit of M_1 and $M_2 \gg 1$ we find that the incompressible χ^{∞}_{eff} is always positive and composition independent (solid line in Figure 2). Small negative values for the incompressible athermal blend χ^{∞}_{eff} can arise with smaller M_1 and M_2 for specific monomer structure pairs. As the excess free volume increases (the pressure is lowered), mixing is facilitated, and χ^{∞}_{eff} develops a composition dependence. Simultaneously χ^{∞}_{eff} becomes increasingly negative. It is finally negative over the whole concentration range for sufficiently large average excess free volume $\bar{\phi}_v$ (≈0.3 for the model in Figure 2).

Since all attractive van der Waals interaction energies ϵ_{ij}/k_BT (i,j = 1, 2) vanish in the idealized athermal blend, relatively high pressures P are necessary either to prevent the excess free volume from becoming unreasonably large and/or to maintain a dense one-phase region. For instance, the model example of Figure 2 yields ϕ_v = 0.37, 0.23, 0.11, and 0.06 for Φ_1 = 0.5 and for P = 1000, 2000, 4000, and 6000 atm, respectively. These ϕ_v values vary with composition Φ_1 by less than 1.2% over the whole range of Φ_1 at constant P and T. Interestingly, the tendency of the effective polymer–polymer interaction χ^{∞}_{eff} to become increasingly attractive as ϕ_v grows parallels exactly a similar tendency in polymer solutions as the concentration of impurities grows.[21]

The effective interaction parameter χ^{∞}_{eff} in Figure 2, defined in terms of the zero-angle coherent scattering functions, can be compared with a similar quantity g^{∞}_{eff} determined directly from the LCT noncombinatorial athermal limit entropy of mixing $\Delta S^{mix}_{nc,\infty}$ as

$$g^{\infty}_{eff} \equiv \frac{-\Delta S^{mix}_{nc,\infty}}{N_l k_B \Phi_1 \Phi_2} \quad (3.13)$$

This athermal effective interaction parameter g^{∞}_{eff} is presented in Figure 3 for the same model binary blend, temperature T, and pressures P as in Figure 2. The g^{∞}_{eff} in Figure 3 is always negative in the one-phase region, decreases monotonically with composition Φ_1, and reaches the incompressible limit with increasing pressure P more rapidly for smaller Φ_1. This behavior of g^{∞}_{eff} differs significantly from that displayed for χ^{∞}_{eff} in Figure 2 and therefore emphasizes the well-known fact that different types of experimental measurements of the effective interaction parameter may result in quite different quantities when the interaction parameter is composition dependent. Similar differences persist for the examples illustrated in Figures 4 and 5.

While molecular weights and monomer structures strongly affect χ^{∞}_{eff} (as shown in Figures 4 and 5 for a P = 1000 atm athermal blend), they have practically no influence on g^{∞}_{eff}. Low molecular weights produce more negative χ^{∞}_{eff} in Figure 4, but simultaneously they magnify the rounding off of the $\chi^{\infty}_{eff}(\Phi_1)$ curves near the pure melt limits, $\Phi_1 \to 0$ or 1. Thus, experiments performed for mixtures of polymer species with much higher molecular weights should not perceive this LCT prediction, which is accentuated in Figure 4 because of the use of a low value for M_i. A very slight change in ϕ_v arises as both of the M_i vary. The overall variation of ϕ_v is less than 1% over the range of M_i = 50–400. This suggests that the behavior for χ^{∞}_{eff} at a given pressure is similar to that at a constant volume when the volume is specified by the average value of ϕ_v at that pressure.

Increased "asymmetry" between the monomer structures of the two components leads to the athermal limit χ^{∞}_{eff} becoming more positive in Figure 5. In the long-chain limit of M_1 and $M_2 \to \infty$, this monomer structure asymmetry factor is defined here as being proportional to

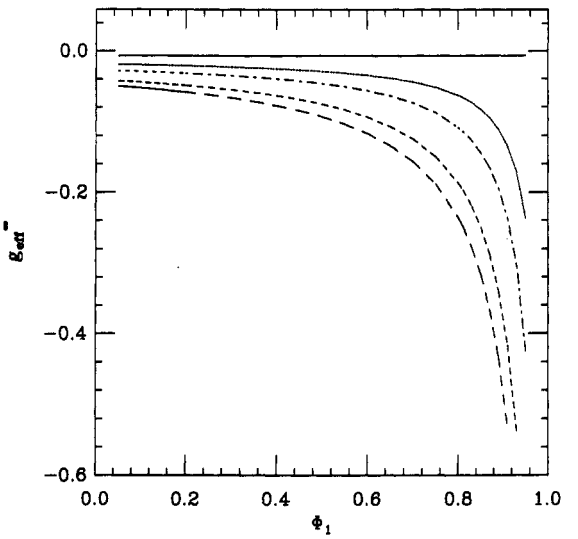

Figure 3. Idealized athermal limit effective interaction parameter $g^{\infty}_{eff}(\Phi_1)$ as determined from the LCT athermal limit noncombinatorial entropy of mixing (see eq 3.13) for the same model blend and pressures as in Figure 2.

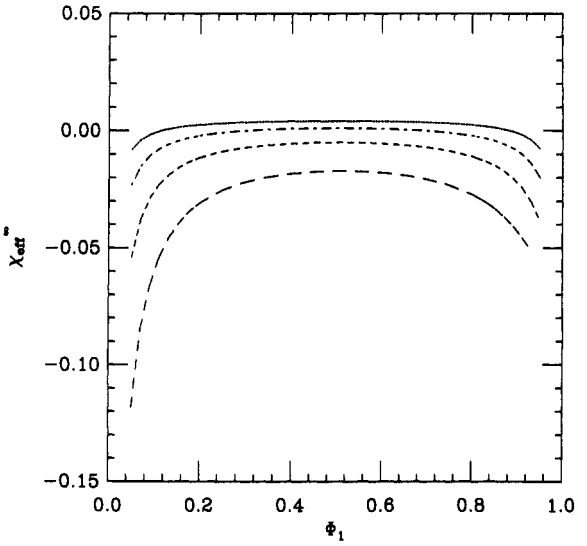

Figure 4. Typical molecular weight dependence of the LCT idealized athermal limit small-angle neutron scattering effective interaction parameter χ^{∞}_{eff} at P = 1000 atm. The curves correspond to $M_1 = M_2$ = 50 (– –), $M_1 = M_2$ = 100 (- - -), $M_1 = M_2$ = 200 (– · –), and $M_1 = M_2$ = 400 (···). Other parameters as given in Figure 2.

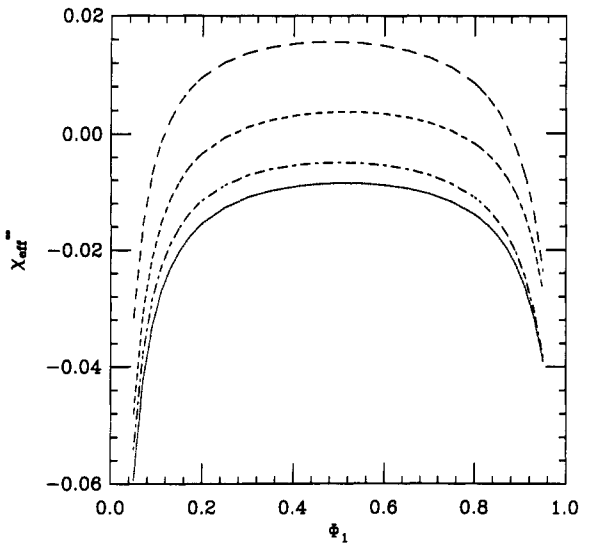

Figure 5. LCT idealized athermal limit small-angle neutron scattering effective interaction parameter $\chi^{\infty}_{eff}(\Phi_1)$ at $P = 1000$ atm for various structured monomer blends. The curves from top to bottom are for a–c, a–e, a–b, and a–d binary blends that are listed in order of increasing asymmetry as defined by eq 3.14. Other parameters are specified in Figure 2.

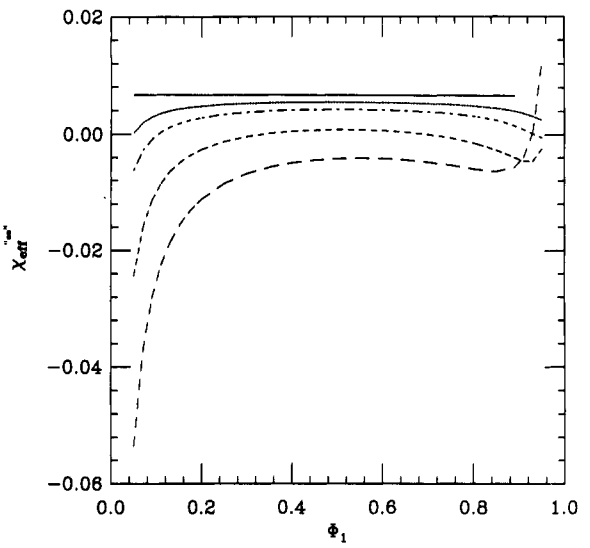

Figure 6. LCT quasi-athermal small-angle neutron scattering effective interaction parameter $\chi^{"\infty"}_{eff}(\Phi_1)$ at $P = 1$ atm for various attractive van der Waals energies $\epsilon_{11} = \epsilon_{22} = \epsilon_{12}$ ($\epsilon \equiv \epsilon_{11} + \epsilon_{22} - 2\epsilon_{12} = 0$, and $\epsilon_{11} = \epsilon_{22} \neq 0$). The curves from top to bottom correspond to $\epsilon_{11}/k_BT = 3.0$, 0.725, 0.58, 0.44, and 0.37.

$$x(1,2) = \left[\frac{N_2^{(1)}}{M_1} - \frac{N_2^{(2)}}{M_2}\right]^2 \tag{3.14}$$

The counting parameters $N_2^{(\mu)}/M_\mu$ are given in ref 4 for structures a–c of Figure 1 and will be provided for a large number of vinyl monomer structures in paper 3. Each of the athermal limit model binary blends, whose χ^{∞}_{eff} at $P = 1000$ atm is presented in Figure 5, consists of one component that involves linear polymers and the other species being one of the branched polymer structures d, b, e, and c of Figure 1 and being listed as follows in order of the increasing asymmetry with respect to structure a as defined by (3.14): $x(d,a) = 1/9$, $x(b,a) = 1/4$, $x(e,a) = 9/16$, and $x(c,a) = 1$. The corresponding void volume fractions are $\phi_v(d,a) = 0.372$, $\phi_v(b,a) = 0.367$, $\phi_v(e,a) = 0.374$, and $\phi_v(c,a) = 0.366$. In contrast to the pressure dependence displayed in Figures 2 and 4 for a single structured monomer blend, Figure 5 does not show a monotonic dependence of χ^{∞}_{eff} on the free volume ϕ_v.

The LCT calculations for the athermal limit neutron scattering χ^{∞}_{eff} (or for the $\chi^{"\infty"}_{eff}$ that are introduced in subsection B below) have the common feature of changing from positive values for an incompressible blend to negative ones for blends with sufficient excess free volume. In contrast, g^{∞}_{eff} for stable binary blends, as defined in terms of the free energy of mixing analogously to (3.13), is negative for all ϕ_v (including $\phi_v = 0$) and does not depend to a significant degree on monomer structures and molecular weights when the M_i are large (for example, 100 in Figure 3). Strong dependences are, however, found in ref 6 for the polymer–solvent system. The general trends in Figures 2–7 apply also for other pairs of monomer structures of Figure 1 with only quantitative changes to χ^{∞}_{eff}, $\chi^{"\infty"}_{eff}$, and g^{∞}_{eff}. Thus, the presence of the free volume enhances miscibility of athermal blends (and makes both χ^{∞}_{eff} and g^{∞}_{eff} more negative). The trend toward decreasing χ^{∞}_{eff} would suggest greater miscibility in the athermal limit as being promoted by smaller molecular weights and greater similarity between the monomer structures of the two blend components. However, the latter conclusion contrasts with the trends displayed by the interaction parameter g^{∞}_{eff}, which has more direct relevance to miscibility than does the χ^{∞}_{eff} from neutron scattering experiments.

It is interesting to compare the LCT predictions for χ^{∞}_{eff} with corresponding calculations of Schweizer and Curro using RISM intergral equation theory.[20] Both theories involve completely different approaches and different models (lattice versus continuum hard-sphere system) and are therefore complementary in nature. As discussed more in the section V, the RISM calculations of Schweizer and Curro have been applied only to compressible systems, but they employ an incompressible limit definition of χ^{∞}_{eff} that significantly departs from ours in (3.1) or (3.2). We find many parallel trends between our calculations of thermodynamic properties and theirs, and the parallelism increases when quantities obtained from LCT are used to evaluate the χ^{∞}_{eff} that is defined by Curro and Schweizer.

B. Realistic Athermal Blend Limit. The examples in Figures 2–5 employ an idealized model for an athermal limit blend that contains no attractive interactions. Such a system is found to produce a stable one-phase blend only at very high pressures (of the order of 10^3 atm). Attractive interactions in real systems provide the cohesive forces that permit stable blends to exist at normal pressures and temperatures. Thus, a more realistic model of an athermal blend requires the presence of attractive interactions. A first guess at such a more realistic model and quasi-athermal polymer blend, which is stable at normal atmospheric pressures and temperatures, is a model binary system with zero exchange energy $\epsilon \equiv \epsilon_{11} + \epsilon_{22} - 2\epsilon_{12} = 0$ and equal, but nonzero self-interaction energies $\epsilon_{11} = \epsilon_{22} \neq 0$. The corresponding effective interaction parameter $\chi^{"\infty"}_{eff}$ is presented in Figure 6 as a function of composition Φ_1 at the constant pressure of $P = 1$ atm and for several values of ϵ_{11}. The general behavior of $\chi^{"\infty"}_{eff}$ is very similar to that illustrated in Figure 2 for the high-pressure athermal limit blend. Quantitative differences emerge mainly for small ϵ_{11} and involve only the region of Φ_1 close to unity, where the rounding occurs because of use of low molecular weights. When ϵ_{11} is sufficiently high, the excess free volume ϕ_v tends to zero even at low pressures; e.g., $P = 1$ atm, and consequently $\chi^{"\infty"}_{eff} \rightarrow \chi^{\infty}_{eff}(P = \infty)$ as ϵ_{11} becomes

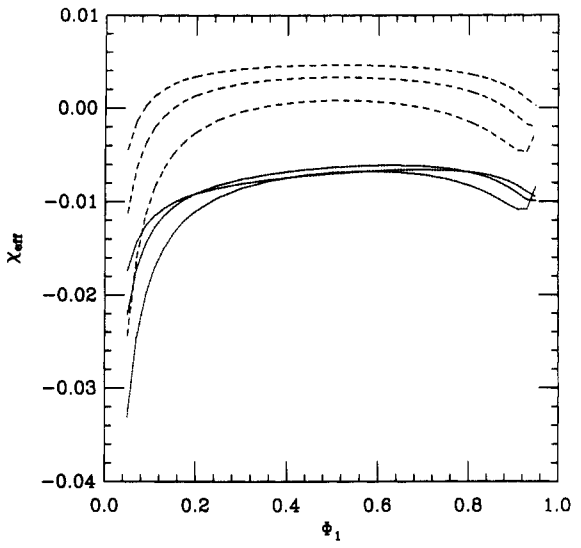

Figure 7. LCT quasi-athermal small-angle neutron scattering effective interaction parameter $\chi_{eff}^{"\infty"}(\Phi_1)$ at $P = 1$ atm (which approaches the incompressible limit of χ_{eff}^{∞} only as $T \to \infty$) for $\epsilon_{11}/k_B = \epsilon_{22}/k_B = 182.87$ K and $\epsilon \equiv \epsilon_{11} + \epsilon_{22} - 2\epsilon_{12} = 0$ at the temperatures 300.15, 350.15, and 415.15 K (dashed lines from top to bottom). Dotted curves show the effective interaction parameter χ_{eff} for a binary blend with the same self-interaction energies $\epsilon_{11}/k_B = \epsilon_{22}/k_B = 182.67$ K, but with nonzero exchange energy $\epsilon/k_B = -2.075$ K. These overlapping dotted curves correspond (from top to bottom on the left-hand side) to the increasing temperatures 300.15, 350.15, and 415.15 K. In spite of the presence of nonzero attractive interaction energies, χ_{eff} is fairly insensitive to temperature, except for compositions close to pure melt limits.

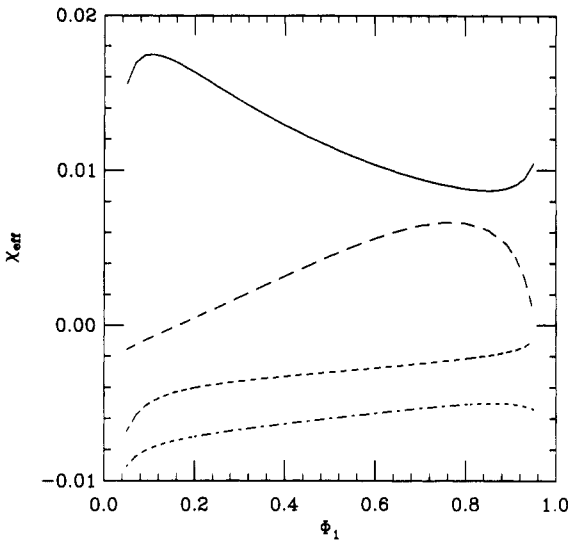

Figure 8. LCT nonathermal small-angle neutron scattering effective interaction parameter $\chi_{eff}(\Phi_1)$ at $P = 1$ atm for various self-interaction energies ϵ_{22} and constant $\epsilon_{11}/k_BT = 1.0$ and $\epsilon/k_BT = -0.007$. The curves correspond to ϵ_{22}/k_BT equal to 0.68 (—), 0.85 (- - -), 1.0 (– · –), and 1.6 (– –).

large. The values of $\epsilon_{11} = \epsilon_{22}$ in Figure 6 are chosen to reproduce the same ϕ_v as in the high-pressure curves $\chi_{eff}^{\infty}(\Phi_1)$ of Figure 2.

The LCT χ_{eff} depend on the reduced interaction energies ϵ_{ij}/k_BT, so variations with ϵ_{ij} and T are effectively interchangeable. Because of the choice $\epsilon = 0$ and $\epsilon_{11} = \epsilon_{22}$, Figure 6 shows simultaneously the influence of temperature T on $\chi_{eff}^{"\infty"}$. As T increases (i.e., ϵ_{11} decreases), $\chi_{eff}^{"\infty"}$ generally becomes more negative. Thus, this model is not quite adequate in describing an "athermal" blend. The resolution of this difficulty is readily found as follows: The rate of change of $\chi_{eff}^{"\infty"}$ is much more rapid for higher T (smaller ϵ_{11}) in Figure 6. Introducing a small negative ϵ compensates for most of the temperature dependence of χ_{eff} and leads to a χ_{eff} that is virtually temperature independent. This more realistic model of athermal blends is possible only for compressibile systems with lower molecular weights and is illustrated in Figure 7 for $\epsilon_{11}/k_B = \epsilon_{22}/k_B = 182.67$ K. The upper dashed curves give the quasi-athermal case of $\epsilon = 0$ and the temperatures 300.15, 350.15, and 415.15 K (top to bottom), while the lower overlapping (dotted), curves correspond to the very small exchange energy $\epsilon/k_B = -2.075$ K, the same $\epsilon_{11} = \epsilon_{22}$, and the same set of temperatures (top to bottom on the left-hand side). These athermal-like conditions exist for a wide range of ϵ_{ii} and different monomer structures, and we anticipate that small differences $|\epsilon_{11} - \epsilon_{22}|$ may also be consistent with a similar temperature independence to χ_{eff}. The above examples demonstrate that the temperature independence of experimental χ_{eff} does not necessarily imply the absence of interactions or the equality of the three independent interaction energies $\epsilon_{11} = \epsilon_{22} = \epsilon_{12}$ when molecular weights are not too high. Paper 4 will show that the $M_1, M_2 \to \infty$ athermal limit requires $\epsilon \approx 0$. The heat of mixing for this quasi-athermal blend in Figure 7 has a minimum value of −5.7 J/(mol of lattice sites), which is comparable to experimental data for blends with weak interactions. Our more realistic model of an athermal blend has not been studied by RISM theory or other methods. The implications of the nontrivial behavior displayed in Figure 7 are discussed further in section V.

C. Nonathermal Compressible Binary Blends. The effective interaction parameter χ_{eff} of nonathermal compressible blends is a function of the three independent interaction energies $\epsilon \equiv \epsilon_{11} + \epsilon_{22} - 2\epsilon_{12}$, ϵ_{11}, and ϵ_{22}. The latter two interactions also affect blend compressibility and excess thermodynamic quantities for compressible systems. The exchange energy ϵ is taken as the small value of $-0.007\ k_BT$ for all the model nonathermal blends considered in this subsection. Empirical polymer melt self-interaction energies ϵ_{11} and ϵ_{22} are of order unity[3] (in units of k_BT), and those chosen in Figures 9–15 lie in the ranges $\epsilon_{11} = 0.44$–1.0 and $\epsilon_{22} = 0.44$–1.6 as an illustration. For given monomer architectures and for fixed M_1, M_2, ϵ, T and $P = 1$ atm, we find a strong dependence of the LCT χ_{eff} on both ϵ_{11} and ϵ_{22}. Some typical examples are presented in Figures 8 and 9, where a wide variety of shapes for the curve of $\chi_{eff}(\Phi_1)$ are generated for a pair of model blends differing only in the self-interaction energies ϵ_{11} (Figure 8) or ϵ_{22} (Figure 9). The computed χ_{eff} are nonmontonic functions of ϕ_v, indicating that the ϵ_{11} and ϵ_{22} have more influence on χ_{eff} than ϕ_v (although ϵ_{11} and ϵ_{22} also affect ϕ_v). The calculated χ_{eff} is found generally (see examples in Figures 8 and 9) to grow algebraically with $|\epsilon_{11} - \epsilon_{22}|$. However, the growth is at different rates and to different limits for the two cases $\epsilon_{11} > \epsilon_{22}$ and $\epsilon_{11} < \epsilon_{22}$. A similar strong influence of the energies ϵ_{11} and ϵ_{22} on the shape of the composition dependence computed for χ_{eff} is likewise found for other monomer structures of Figure 1. This feature indicates that the LCT describes a rich variety of behaviors for compressible blends. Higher values of $|\epsilon|$ lead to χ_{eff} being much less sensitive to variations of ϵ_{11} and ϵ_{22}.

Generally, monomer structure does not change the shapes of the χ_{eff} (Φ_1) curves in Figure 8 and 9, but molecular weights can modify χ_{eff} profoundly. The few examples in Figure 10 indicate the mainly quantitative variations with different blend architectures. Figure 11 shows how a roughly parabolic dependence of χ_{eff} on composition Φ_1 for small molecular weights converts

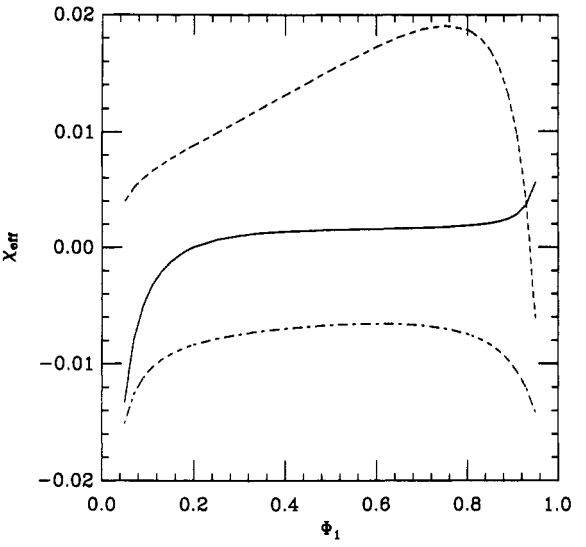

Figure 9. The same as Figure 8, but for constant $\epsilon/k_BT = -0.007$ and $\epsilon_{11}/k_BT = 0.6$ and for various ϵ_{22}/k_BT given by 0.5 (—), 0.65 (- · -), and 0.9 (- - -).

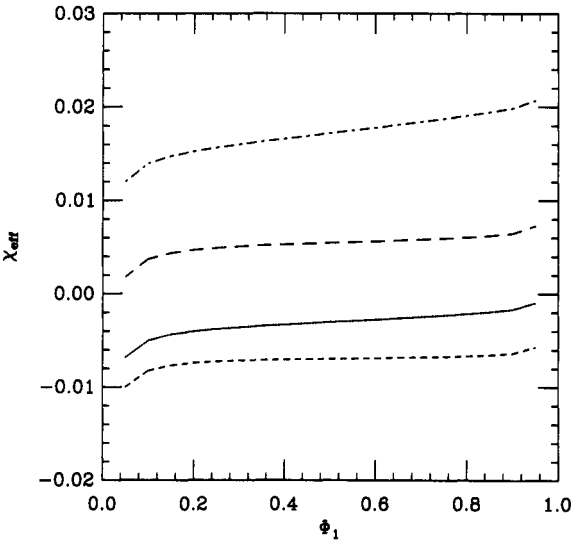

Figure 10. LCT small-angle neutron scattering effective interaction parameter $\chi_{eff}(\Phi_1)$ at $P = 1$ atm for different model monomer structure nonathermal, compressible polymer blends. The energies are $\epsilon/k_BT = -0.007$, $\epsilon_{11}/k_BT = 1.0$, and $\epsilon_{22}/k_BT = 0.85$. The curves (top to bottom) involve *a*–*c*, *a*–*e*, *a*–*b*, and *a*–*d* model blends. The general trend is analogous to that in Figure 5 for χ_{eff}^{∞}.

gradually into a linear function $\chi_{eff}(\Phi_1)$ with increasing molecular weights. Values of M_1 and M_2 of $\sim 10^4$ are necessary to eliminate rounding off of the $\chi_{eff}(\Phi_1)$ curves in Figure 11; our use of lower M_i is to emphasize the short-chain corrections that may appear and that may be useful in empirically determining three independent interaction energies. The blend stability condition 3.11 does not admit of such high values of M_i for the idealized athermal limit blends, and therefore the composition dependence of χ_{eff} remains roughly parabolic (see Figure 4) in this specialized limit. However, more general shapes of $\chi_{eff}(\Phi_1)$ and wider ranges of M_i become possible for our model of a realistic "athermal" blend with attractive interactions present.

An important feature of the LCT, mentioned earlier in connection with athermal blends, lies in the possibility for studying how pressure influences the effective interaction parameter χ_{eff}. Figure 12 displays χ_{eff} for two model blends with identical monomer structures, identical respective site occupancy indexes M_1 and M_2, and energy

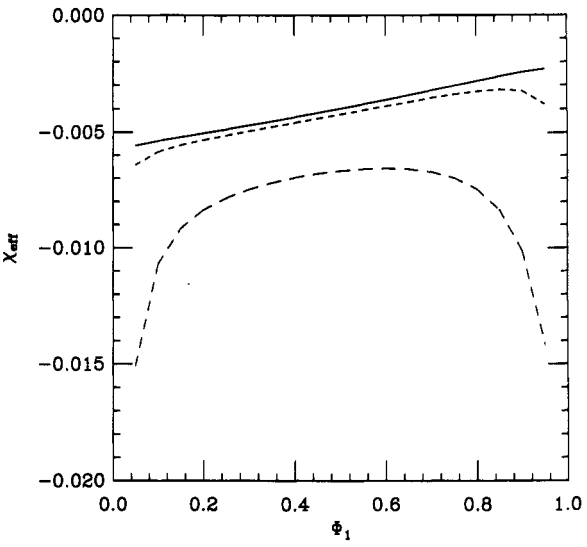

Figure 11. Molecular weight dependence of the LCT nonathermal small-angle neutron scattering effective interaction parameter $\chi_{eff}(\Phi_1)$ at $P = 1$ atm. The site occupancy indexes vary from $M_1 = M_2 = 100$ (long-dashed parabolic curve) to $M_1 = M_2 = 10^4$ (solid linear line). The short-dashed line corresponds to $M_1 = M_2 = 10^3$. The microscopic interaction energy parameters are $\epsilon/k_BT = -0.007$, $\epsilon_{11}/k_BT = 0.6$, and $\epsilon_{22}/k_BT = 0.65$.

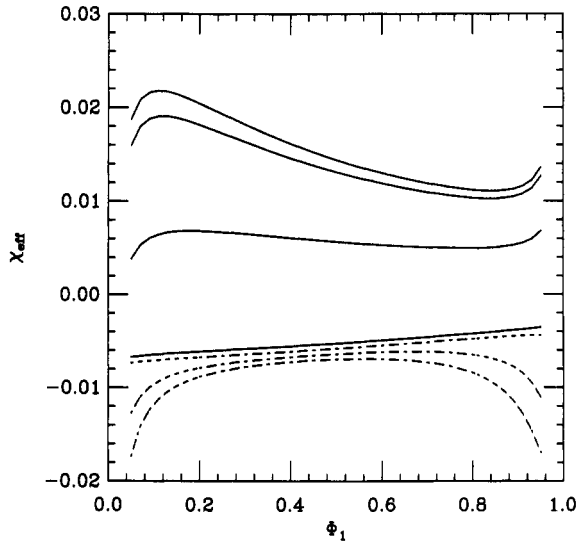

Figure 12. Pressure dependence of the LCT small-angle neutron scattering effective interaction parameter $\chi_{eff}(\Phi_1)$ for two polymer blends as a function of the self-interaction energies, ϵ_{11} and ϵ_{22}. The exchange energy ϵ is identical for both blends and equal to $-0.007\ k_BT$. Solid (upper) curves correspond to blend 1 with $\epsilon_{11}/k_BT = 0.875$ and $\epsilon_{22}/k_BT = 0.6$ at the pressures $P = 1$, 10^2, 10^3, and 10^4 atm (top to bottom). Dashed (lower) curves give $\chi_{eff}(\Phi_1)$ for blend 2 with $\epsilon_{11}/k_BT = 0.55$ and $\epsilon_{22}/k_BT = 0.6$ at $P = 1$, 10^3, and 10^4 atm. The figure shows that variations of χ_{eff} with pressure P may occur in both directions. Both model blend χ_{eff} approach the $P \to \infty$ incompressible limit of χ_{eff} which for given T, M_i and monomer structures depends only on the exchange energy $\epsilon \equiv \epsilon_{11} + \epsilon_{22} - 2\epsilon_{12}$.

parameter ϵ, but different self-interaction energies ϵ_{11} and ϵ_{22}, respectively. When the pressure increases from 1 to 10^4 atm, χ_{eff} for blend 1 decreases (solid curves in Figure 12) toward the incompressible limit. On the other hand, χ_{eff} for blend 2 increases (dashed curves in Figure 12). At a pressure of $P = 10^4$ atm the composition dependence of χ_{eff} becomes linear for both blends, and the incompressible limit χ_{eff}^{∞} depends only on ϵ, M_1 and M_2, but no longer on ϵ_{11} and ϵ_{22} separately. An increasing pressure P always makes χ_{eff} become closer to the incompressible limit χ_{eff}^{inc}. Thus, it is the relative values of χ_{eff} at pressure P and

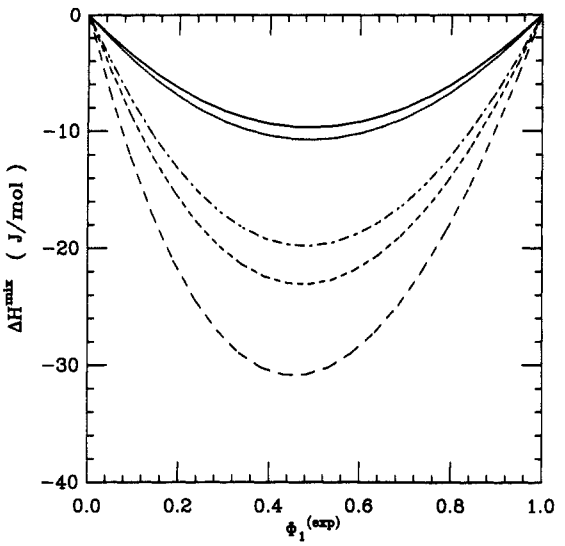

Figure 13. Typical pressure dependence of the heat of mixing $\Delta H^{mix}(\Phi_1^{(exp)})$ [expressed here in J/(mol of lattice sites)] at T = 373.15 K. The curves are as follows: - - (1 atm), - - - (500 atm), - · - (10^3 atm), ··· (10^4 atm), and — ($P \to \infty$, i.e., incompressible limit). The interaction energies are the same as those represented for blend 1 in Figure 12.

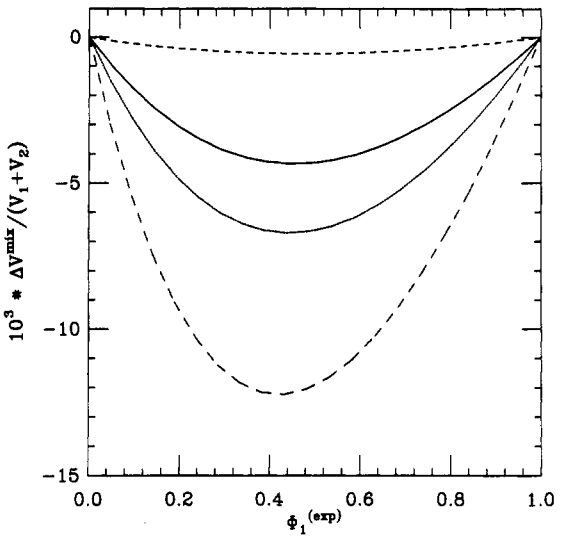

Figure 14. The same as Figure 13 for $\Delta V^{mix}/(V_1 + V_2)$. The curves are as follows: - - (P = 1 atm), ··· (P = 500 atm), — (P = 1000 atm), and - - - (P = 5000 atm).

its high-pressure limit that determines whether a given χ_{eff} grows or diminishes with increasing P.

Nonathermal blends yield an effective interaction parameter χ_{eff} that, except for the special case illustrated in Figure 7, must be temperature dependent. Classic FH theory describes χ_{eff} in terms of only one energy parameter ϵ, as a linear function of the inverse temperature $1/T$, and as independent of the monomer molecular structures. The incompressible LCT, on the other hand, provides a wealth of different $\chi_{eff}(1/T)$ curves whose forms vary with monomer architectures and obviously with three reduced energy parameters ϵ/k_BT, ϵ_{11}/k_BT, and ϵ_{22}/k_BT. Large deviations from a linear variation of the LCT χ_{eff} with $1/T$ appear mostly because of the use of small M_i. Some deviations persist due to the second-order energy contributions from Table I. We shall consider the temperature dependence of χ_{eff} in more detail in the following paper describing the LCT predictions for PS/PVME blends. Hence, this point is not discussed further here. Suffice it to say that the shape of $\chi_{eff}(\Phi_1)$ may be altered by changes in temperature.

Sariban and Binder[22] have performed Monte Carlo simulations of the lattice model for blends of linear chains with $M_1 = M_2$ and $\phi_v = 0.2$. In order to simplify matters, they take $\epsilon_{11} = \epsilon_{22} = 0$, but permit ϵ to be nonzero. Our LCT calculations show that the pressure of such systems is greater than 10^3 atm, again stressing the need for using all three independent interaction energies to study properties of real polymer systems under normal conditions.

IV. Heat of Mixing ΔH^{mix} and Volume of Mixing ΔV^{mix} for Compressible Binary Blends

The LCT enables a determination of other blend thermodynamic properties, Figures 13 and 14 present the heat of mixing and the volume of mixing, respectively, as a function of composition for various values of the pressure. The model blend is the same as that used to compute the upper (solid) curves in Figure 12. The (absolute value of the) heat of mixing in Figure 13 decreases with pressure and reaches the incompressible limit for $P > 10^4$ atm. The volume of mixing ΔV^{mix} in Figure 14 is a more asymmetrical function of composition Φ_1 than is ΔH^{mix}. Figure 14 shows how ΔV^{mix} approaches zero in the $P = \infty$ limit of an incompressible blend and increases (in absolute value) with a decrease in pressure. The dependence of ΔH^{mix} and ΔV^{mix} on pressure P does not change qualitatively with monomer molecular structures. For example, the changes in ΔH^{mix} at P = 1 atm do not exceed 30% when the branched structure b in the model blend of Figure 13 is replaced by another branched structure d. Monomer structure influences the heat of mixing ΔH^{mix} through changes in contact probabilities and through its influence on the excess free volume fraction ϕ_v. The latter, in turn, is mostly affected by the energy parameters ϵ_{11} and ϵ_{22}. Since introducing voids removes favorable polymer–polymer contacts and thereby must cost energy, small values of ϵ_{11} and ϵ_{22} facilitate larger excess free volumes. Greater differences between ϵ_{11} and ϵ_{22} promote increased ΔV^{mix} and, therefore, somewhat affect ΔH^{mix}. Comparison of the effective interaction parameter $\chi_{eff}(\Phi_1)$ in Figures 8 and 9 with $\Delta H^{mix}(\Phi_1)$ and $\Delta V^{mix}(\Phi_1)$ for the same systems (not presented here) shows that more positive χ_{eff} correspond to more negative ΔH^{mix} and ΔV^{mix}. The variations in χ_{eff} and ΔH^{mix} (or ΔV^{mix}) with ϵ_{11} and ϵ_{22} are in opposite directions, a feature that is generally found for the LCT computations of compressible binary blends with a small exchange energy ϵ. An increase in temperature reduces the free volume and diminishes the absolute values of the heat of mixing ΔH^{mix}. This behavior presented in Figure 15 agrees qualitatively with that resulting from our LCT calculations[6] for incompressible polymer–solvent systems. Generally, temperature affects ΔH^{mix} for compressible systems through its influence on the free volume, and therefore the dependence of $\Delta H^{mix}(\Phi_1)$ on the temperatures depicted in Figure 15 is as expected.

We may define a nonathermal effective interaction parameter g_{eff} from the heat of mixing ΔH^{mix} as

$$g_{eff} = \frac{\Delta H^{mix}}{N_l k_B T \Phi_1 \Phi_2} \tag{4.1}$$

This g_{eff} for compatable blends with negative ϵ is always negative and is linearly dependent on composition Φ_1 over the whole range of pressures P (see Figure 16). The behavior displayed in Figure 16 thus differs from the purely entropic g_{eff}^{∞} depicted in Figure 3. Molecular weights and monomer molecular structures weakly affect the magnitude of g_{eff}, while their influence on g_{eff}^{∞} is practically not noticeable. Since thermodynamic miscibility depends on

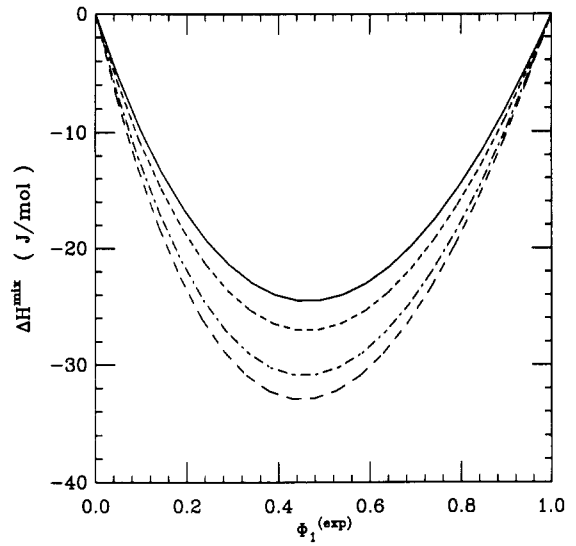

Figure 15. Typical temperature dependence of the heat of mixing $\Delta H^{mix}(\Phi_1^{(exp)})$ at P = 1 atm. The microscopic interaction parameters are chosen as $\epsilon/k_B = -2.91$ K, $\epsilon_{11}/k_B = 363.26$ K, and $\epsilon_{22} = 249.09$ K. The curves from top to bottom correspond to T = 293.15, 323.15, 373.15, and 403.15 K.

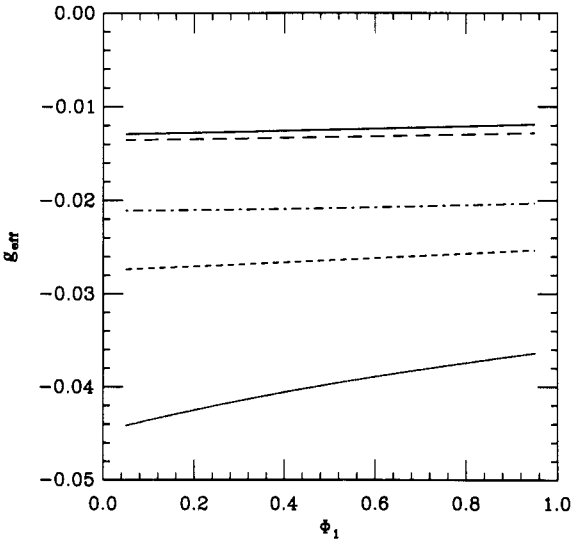

Figure 16. Typical pressure dependence of the effective interaction parameter $g_{eff}(\Phi_1)$ determined from the heat of mixing ΔH^{mix} (see eq 4.1) for a model binary blend with $\epsilon/k_BT = -0.007$, $\epsilon_{11}/k_BT = 0.875$, and $\epsilon_{22}/k_BT = 0.6$. The curves from top to bottom correspond to P = ∞, 5000, 1000, 500, and 1 atm.

ΔH^{mix}, the interaction parameter g_{eff} is more relevant than χ_{eff} to studies of blend miscibility. The examples presented here indicate that the small-angle neutron scattering χ_{eff} can depart qualitatively from g_{eff}, especially when ϵ is quite small. Thus, χ_{eff} may provide a poor measure of blend compatability or incompatability. This feature has been accentuated here by our use of a small ϵ since differences between the behavior or χ_{eff} and g_{eff} diminish when $|\epsilon|$ increases. Nevertheless, χ_{eff} appears to be the most sensitive to monomer structure, reflecting the utility of neutron scattering experiments in probing molecular structure and interactions.

V. Discussion

The lattice cluster theory is generalized in the preceding paper to multicomponent, compressible mixtures of polymers with arbitrary molecular structure. This LCT is shown here to describe the thermodynamic properties for a rich range of polymer systems. The illustrations of the LCT predictions in sections III and IV are specialized to the small-angle neutron scattering (SANS) Flory effective interaction parameter χ_{eff}, the heat of mixing ΔH^{mix}, and the volume of mixing ΔV^{mix} of a compressible binary blend, but a wide variety of other thermodynamic properties are readily obtained from the LCT free energy expressions in Table I. The figures in sections III and IV delineate variations of blend properties with composition, pressure, interaction energies ϵ_{ij}, and monomer molecular structures. They show several quantitatively different composition dependences of χ_{eff} as well as the experimentally unexplored pressure dependence of χ_{eff}. Generally, increasing pressure reduces ϕ_v and contributions associated with ΔV^{mix}, so some of the general trends are simply understood physically. Our illustrations are not meant to be exhaustive, but are designed to indicate how the theory may be employed.

The athermal limit entropic contribution χ_{eff}^{∞} to the effective interaction parameter has been an enigmatic quantity for many years, but its molecular origins may now be studied within the LCT. Beginning with the simplest incompressible athermal limit, we find that χ_{eff}^{∞} in the long-chain limit of M_1, $M_2 \to \infty$ is positive and is determined by

$$\chi_{eff}^{\infty} = \frac{1}{z^2}\left[\frac{N_2^{(1)}}{M_1} - \frac{N_2^{(2)}}{M_2}\right]^2 \tag{5.1}$$

where $N_2^{(\mu)}$ represents the number of successive bond pairs in a single chain of species μ. Compressibility and finite molecular weights diminish χ_{eff}^{∞} toward negative values, and χ_{eff}^{∞} may even be negative over the whole composition range for sufficiently large ϕ_v or equivalently low pressure. An incompressible athermal blend composed of two identical polymer species with the same polymerization indexes has $\chi_{eff}^{\infty} = 0$ in the large M_i limit. However, the presence of free volume ($\phi_v \neq 0$) in the compressible system introduces density fluctuations, which coherently scatter neutrons, etc. Consequently, we have $\chi_{eff}^{\infty} \neq 0$. The right side of eq 5.1 is a measure of blend asymmetry, which hinders blend miscibility. Other hindrances to miscibility are high molecular weights and the lack of free volume. The latter arises for higher pressures, but contributions to χ_{eff}^{∞} also emerge from ΔV^{mix}.

SANS experiments on polymer blends find that the effective interaction parameter χ_{eff} is temperature independent for certain systems.[19,23] A common thermodynamic interpretation of this χ_{eff} is based on the incompressibility assumption, which leads, in turn, to a vanishing exchange energy $\epsilon \equiv \epsilon_{11} + \epsilon_{22} - 2\epsilon_{12} = 0$ for the athermal case. Hence, this χ_{eff} is considered as a quantity of purely entropic origin. Our results depicted in Figure 7 reveal that the temperature insensitivity of χ_{eff} can also arise for lower molecular weight compressible systems with the presence of the three attractive interaction energies: equal (or slightly differing) values of ϵ_{11} and ϵ_{22}, with ϵ_{12} comparable to them. Blend stability at normal pressures and temperatures implies that none of the ϵ_{ij} vanishes and that ϵ, therefore, need not vanish. This system defines the quasi-athermal case which, we believe, more closely reflects reality than the purely athermal system with all $\epsilon_{ij} = 0$. Thus, the temperature insensitivity of experimental small-angle neutron scattering interaction parameter χ_{eff} for low molecular weight blends[24] does not imply the absence of attractive interactions or their cancellations through $\epsilon = 0$. RISM calculations[20] employ a hard-sphere model for athermal blends with only repulsive forces. Our computations suggest that these model systems would yield

stable blends only at elevated pressures. Thus, the agreement of the RISM theory predictions with some experimentally found linear composition dependences of small-angle neutron scattering χ_{eff}^{∞} may therefore not be totally applicable to the actual systems. Other remarks concerning the RISM definition of χ_{eff} are described in detail below.

A compressible polymer system permits the introduction of several different macroscopic interaction parameters: χ_{eff} is defined in terms of the small-angle neutron scattering structure factor, while g_{eff} is derived from the Gibbs free energy of mixing (or the heat of mixing ΔH^{mix}) (see eqs 3.13 and 4.1). These macroscopic interaction parameters have different values and exhibit varying behaviors as a function of molecular parameters and thermodynamic state variables. A strong dependence of χ_{eff} on molecular monomer structures is contrasted with a very weak sensitivity of g_{eff} to molecular weights and architectures of the two blend components. Certainly, the interaction parameter g_{eff} is a more precise measure of blend miscibility, while the interaction parameter χ_{eff} is a useful quantity for determination of blend spinodals at constant volume. Numerous LCT calculations show that the changes of χ_{eff} and the heat of mixing ΔH^{mix} with variations ϵ_{11} and ϵ_{22} may proceed in opposite directions.

Since the zero-angle coherent scattering structure factor $S_{11}(0)$ depends considerably on molecular monomer structure, we expect a similar behavior for $S_{11}(k \neq 0)$ because this partial structure factor depends on three independent effective macroscopic interaction parameters that vary with monomer structure (all else remaining constant). We plan to study this dependence of $S_{11}(k \neq 0)$ on molecular architecture, pressure, etc., in a future paper.

As described in paper 1, the LCT is amenable to systematic improvements. Foremost among those are the description of the entropy associated with the distribution of the free volume. Equation of state[10] and Dickman–Hall[2]-type models are more realistic in this regard and should be used in quantitative discussion of pressure dependences. However, we have used the simpler lattice model form $\phi_v \ln \phi_v$ which is adequate for exhibiting the interesting general trends.

The general dependence of macroscopic interaction parameters, such as χ_{eff} or g_{eff}, on composition leads to difficulties when empirical values of the interaction parameter are used in theories to predict interfacial profiles, coexistence curves, etc., as it is necessary to specify the precise composition for which the effective parameter should be inserted into prior theory with composition-independent χ_{eff} as well as the particular experimental method that should be used for determining the proper parameter. An interesting illustration of this point is provided in recent computations by Tang and Freed[14] of interfacial widths and tensions in phase-separated binary blends where large errors in these properties may be incurred due to neglecting the composition dependence of χ_{eff} and g_{eff} or due to using one of these quantities at an inappropriate composition in a theory with composition independent χ_{eff}.

There is an interesting analogy between impurities introduced[21] into polymer solutions and voids that represent the excess free volume in the LCT models of blends. Both impurities and voids lead to increasingly attractive effective polymer–polymer interactions. This, in turn, produces a decrease in the critical temperature of polymer blends and facilitates miscibility.

We return now to a comparison of the athermal limit effective interaction parameter χ_{eff}^{∞} provided by the lattice cluster theory and that obtained from the RISM integral equation theory of Schweizer and Curro.[20] Both theories start from different models of a real polymer blend. The RISM theory employs a continuum model in which polymer monomers are represented by hard spheres. (The nonathermal case is described by additional attractive interactions with Lennard-Jones potentials.) Various monomer structures differ only in the hard-sphere diameters and intersphere separations. The blends are always taken to be compressible as $V - V^* > 0$ in their model. Close-packed hard spheres have a packing fraction η of $\sim$67%, while the RISM computations of χ_{eff}^{∞} are carried out for η in the range of 0.45–0.5, corresponding in the lattice model of athermal blends to excess free volumes of ϕ_v = 0.25–0.33 and substantial pressures.

The LCT and RISM theories are generally in agreement for χ_{eff}^{∞}. For instance, they both predict negative χ_{eff}^{∞}, which increases in absolute value with smaller molecular weights. On the other hand, there are some apparent differences. RISM theory yields a linear dependence of χ_{eff}^{∞} (χ_S in their notation) on composition Φ_1, while the LCT curves for $\chi_{eff}^{\infty}(\Phi_1)$ curves exhibit the parabolic convex-up shapes displayed in Figures 2, 4, and 5. A further apparent disagreement concerns the influence of blend density and structural asymmetry. Figures 2 and 4 of section III show that miscibility (i.e., as suggested by more negative χ_{eff}^{∞}) is promoted by a larger excess free volume ϕ_v and a larger similarity of two polymer species. Exactly the reverse conclusions emerge from RISM calculations. As described below, we ascribe the above apparent discrepancies to different definitions of the χ_{eff}^{∞} used by LCT and RISM theory. The differences between models (lattice versus continuum hard-sphere system) are much less important.

RISM theory is used by Schweizer and Curro to compute approximate structure factors $S_{\alpha\beta}(k)$, α, β = 1, 2, for scattering by α–β monomer pairs in a compressible blend. Influenced by the common utilization of the incompressible RPA[18] to extract χ_{eff} from experimental small-angle neutron scattering structure factors $S(k)$, Schweizer and Curro introduce an incompressibility condition to define their χ_S, which we now demonstrate differs from our (3.1) or (3.3). The authors first define the inverse of a total incompressible-like structure factor $S_c(k)$ as a linear combination of the $S_{\alpha\beta}^{-1}(k)$

$$\frac{\rho}{S_c(k)} = S_{11}^{-1}(k) + S_{22}^{-1}(k) - 2S_{12}^{-1}(k) \tag{5.2}$$

where ρ denotes the total monomer density number and where, for simplicity, we quote the case of equal monomeric volumes. The effective interaction parameter χ_S is then defined by Schweizer and Curro in terms of $S_c(0)$ as

$$\chi_S = -\frac{1}{2}\left[S_c(0)^{-1} - \frac{1}{M_1\Phi_1} - \frac{1}{M_2\Phi_2}\right] \tag{5.3}$$

Expressions 5.2 and 5.3 differ from χ_{eff} of (3.3), (3.6), or that which adequately describes experiments in which the scattering contrast is not complete. If p_α represents the scattering length for species α, then the experimental $S(0)$ is defined by

$$(p_1 - p_2)^2 S(0) \equiv p_1^2 S_{11}(0) + p_2^2 S_{22}(0) + 2p_1 p_2 S_{12}(0) \tag{5.4}$$

The idealized limit of perfect contrast sets $p_2 = 0$ in (5.4) and reduces the common empirical definition of χ_{eff} to that used in eqs 3.1 and 3.3.

In order to demonstrate that the majority of discrepancies between LCT and RISM calculations arises from the differing definitions for our χ_{eff} and their χ_S, we have

inserted LCT quantities into their expression for χ_S. The latter emerges from RISM theory as a function of the Fourier transform of the Orstein–Zernike direct intermolecular correlation functions $C_{11}(0)$, $C_{22}(0)$, and $C_{12}(0)$ as

$$\chi_S \approx [R^{-1}C_{11}(0) + RC_{22}(0) - 2C_{12}(0)] \qquad (5.5)$$

where R is the ratio of monomer volumes. Thus, in order to compute χ_S from the LCT, it is necessary to find the correspondence between the thermodynamic quantities $C_{\alpha\beta}(0)$ of RISM theory and quantities that may be evaluated from the composition-dependent $g_{\alpha\beta}$ appearing in the LCT representation of the noncombinatorial portion of the Helmholtz free energy of mixing, which in Table I is represented in the compact form

$$\frac{\Delta F_{nc}^{mix}}{N_t k_B T} = \phi_1\phi_2 g_{12} + \phi_1\phi_v g_{11} + \phi_2\phi_v g_{22} \qquad (5.6)$$

This correspondence may be established by evaluating the zero-angle partial structure factors $S_{11}(0)$, $S_{22}(0)$, and $S_{12}(0)$ from the general eq 3.7 with Table I and then by equating them, respectively, to the RISM $S_{\alpha\beta}(0)$ that are given by eqs 2.16–2.18 of ref 20. After some algebra, the correspondence is found to be

$$C_{11}(0) = 2g_{11} - \frac{1}{\phi_v} + 2\frac{\partial g_{11}}{\partial \phi_1}(\phi_1 - \phi_v) - \frac{\partial^2 g_{11}}{\partial \phi_1^2}\phi_1\phi_v - 2\frac{\partial g_{12}}{\partial \phi_1}\phi_2 - \frac{\partial^2 g_{12}}{\partial \phi_1^2}\phi_1\phi_2 \qquad (5.7)$$

$$C_{22}(0) = 2g_{22} - \frac{1}{\phi_v} + 2\frac{\partial g_{22}}{\partial \phi_2}(\phi_2 - \phi_v) - \frac{\partial^2 g_{22}}{\partial \phi_2^2}\phi_2\phi_v - 2\frac{\partial g_{12}}{\partial \phi_2}\phi_1 - \frac{\partial^2 g_{12}}{\partial \phi_2^2}\phi_1\phi_2 \qquad (5.8)$$

$$C_{12}(0) = g_{12} - g_{11} - g_{22} + \frac{1}{\phi_v} + \phi_1\left[\frac{\partial g_{12}}{\partial \phi_1} - \frac{\partial g_{11}}{\partial \phi_1}\right] - \phi_2\left[\frac{\partial^2 g_{11}}{\partial \phi_1^2}\right] \qquad (5.9)$$

thereby permitting us to calculate the Schweizer–Curro χ_S from (5.5) in terms of the LCT $g_{\alpha\beta}$ from Table I.

An example of the LCT computations of the Schweizer–Curro χ_S is presented in Figure 17 for a model athermal limit blend. A linear dependence of χ_S on Φ_1 emerges when the $C_{\alpha\beta}(0)$ are determined by eqs 5.7–5.9 and are substituted into eq 5.4. This is in general agreement with RISM computations and confirms the above suggestion that the discrepancies between the LCT and the RISM theory predictions arise mainly from the different definitions of χ_{eff} and disappear when the same definition is used in both theories. We believe that our definition of χ_{eff} more faithfully parallels the one used by the neutron scatering experimentalists who measure partial structure factors for a compressible system but apply the conventional RPA analysis only in effectively *defining* the macroscopic interaction parameter χ_{eff} as in (3.1) or (3.3). It is, however, trivial to substitute RISM calculations of $C_{\alpha\beta}(0)$, obtained for a compressible system, into the general RISM equations for the zero-angle partial structure factors $S_{\alpha\beta}(0)$ in order to evaluate a χ_{eff} that corresponds to the experimental analysis. The inclusion of partial contrast is likewise trivial for both LCT and RISM treatments, and we look forward to further comparisons between predictions of these two complementary theories of polymer fluids.

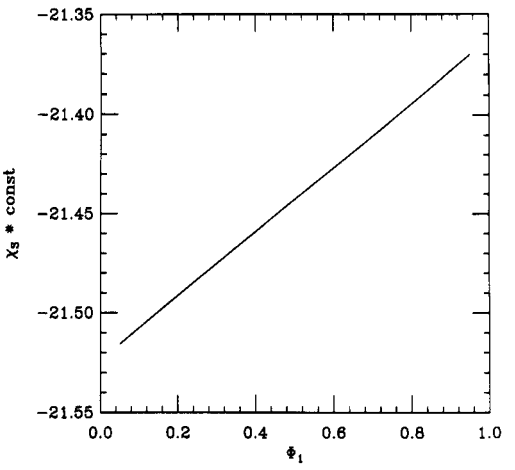

Figure 17. RISM athermal limit effective interaction parameter χ_S (see eq 5.5) as calculated from eqs 5.7–5.9 in terms of the LCT quantities g_{ij}. The model blend involves chains with structures *a–d* of Figure 1, with site occupancy indexes $M_1 = 200$ and $M_2 = 300$, and with the excess free volume $\phi_v = 0.33$. This model corresponds roughly to a hard-sphere blend with packing fraction $\eta = 0.45$, monomer size ratio $\gamma = 1.2$, and $N = 200$, as illustrated in Figure 1 of ref 20.

Acknowledgment. This research is supported, in part, by NSF Grant DMR 89-19941. M.S.F. is grateful for a REU grant from NSF.

References and Notes

(1) Flory, P. J. *J. Chem. Phys.* **1942**, *9*, 660; *Principles of Polymer Chemistry*; Cornell University Press: Ithaca, NY, 1953. Huggins, M. L. *J. Chem. Phys.* **1941**, *9*, 440; *J. Phys. Chem.* **1942**, *46*, 151; *Ann. N.Y. Acad. Sci.* **1943**, *44*, 431.
(2) Dickman, R.; Hall, C. K. *J. Chem. Phys.* **1986**, *85*, 3023.
(3) Sanchez, I. C.; Lacombe, R. H. *Macromolecules* **1978**, *11*, 1145. Sanchez, I. C. *Annu. Rev. Mater. Sci.* **1983**, *13*, 387.
(4) Nemirovsky, A. M.; Bawendi, M. G.; Freed, K. F. *J. Chem. Phys.* **1987**, *86*, 7272.
(5) Freed, K. F.; Bawendi, M. G. *J. Phys. Chem.* **1989**, *93*, 2194, and the references therein.
(6) Dudowicz, J.; Freed, K. F.; Madden, W. G. *Macromolecules* **1990**, *23*, 4803.
(7) Bawendi, M. G.; Freed, K. F. *J. Chem. Phys.* **1987**, *86*, 3720.
(8) Bawendi, M. G.; Freed, K. F. *J. Chem. Phys.* **1988**, *88*, 2741.
(9) Pesci, A. I.; Freed, K. F. *J. Chem. Phys.* **1989**, *90*, 2003.
(10) Flory, P. J. *Discuss. Faraday Soc.* **1970**, *49*, 7. Patterson, D.; Delmas, G. *Discuss. Faraday Soc.* **1970**, *49*, 98.
(11) Dee, G. M.; Walsh, D. J. *Macromolecules* **1988**, *21*, 811, 815.
(12) Dudowicz, J.; Freed, K. F. *Macromolecules* **1990**, *23*, 1519.
(13) Dudowicz, J.; Freed, K. F. *Macromolecules*, preceding article in this issue.
(14) Tang, H.; Freed, K. F. *J. Chem. Phys.* **1991**, *94*, 6307.
(15) Mayer, J. E.; Mayer, M. G. *Statistical Mechanics*; Wiley: New York, 1940.
(16) Guggenheim, E. A. *Mixtures*; Oxford University Press: Oxford, U.K., 1952. Progogine, I. *The Molecular Theory of Solutions*; North-Holland: Amsterdam, 1957.
(17) Han, C. C.; Baurer, B. J.; Clark, J. C.; Muroga, Y.; Okada, M.; Tran-Cong, Q.; Sanchez, I. C. *Polymer* **1988**, *29*, 2002. Bates, F. S.; Muthukumar, G. D.; Wignall, G. D.; Fetters, L. J. *J. Chem. Phys.* **1988**, *89*, 535.
(18) de Gennes, P. G. *Scaling Concepts in Polymer Physics*; Cornell Press: Ithaca, NY, 1979.
(19) Ito, H.; Russell, T. P.; Wignall, G. D. *Macromolecules* **1987**, *20*, 2214.
(20) Schweizer, K. S.; Curro, J. G. *J. Chem. Phys.* **1989**, *91*, 5059.
(21) Edwards, S. F.; Muthukumar, M. *J. Chem. Phys.* **1988**, *89*, 2435. Douglas, J. F. *Macromolecules* **1988**, *21*, 3515. Muthukumar, M. *J. Chem. Phys.* **1989**, *90*, 4594. Cherayil, B. J.; Scheraga, H. A. *Phys. Lett. A* **1989**, *139*, 175. Thirumalai, D. *Phys. Rev. A* **1988**, *37*, 269. Duplantier, B. *Phys. Rev. A* **1988**, *38*, 3647.
(22) Sariban, A.; Binder, K. *J. Chem. Phys.* **1987**, *86*, 5859.
(23) Bates, F. S.; Hartney, M. *Macromolecules* **1985**, *18*, 2478.
(24) Paper 4: Freed, K. F.; Dudowicz, J. *Theor. Chim. Acta*, in press.